ARCHIVES
of
FOUNDRY ENGINEERING

Published quarterly as the organ of the Foundry Commission of the Polish Academy of Sciences

Simulation of the Effect of Impurities in Recycled Silicon Used for the for the Production of Ferrosilicon

P. Padhamnath *, P. Migas, M. Karbowniczek
AGH University of Science and Technology, Poland
* Corresponding author: E-mail address: ppadhamnath@agh.edu.pl

Received 19.09.2024; accepted in revised form 10.01.2025

Abstract

Decarbonization of steel making and allied processes have been receiving immense attention of researchers. Similarly, recycling of waste resources and conversion or recovery of useful materials from waste destined for landfills to mitigate environmental impact, is also an important area of research. Ferrosilicon (FeSi) is currently produced using carbothermic reduction and an energy intensive process. However, silicon (Si) from electronic wastes could be combined with scrap steel to produce FeSi. The Si from electronic waste will, however, contain some impurities such as Aluminium (Al), copper (Cu) and Tin (Sn), which could be incorporated into the FeSi produced from such Si. Hence, in this work the impact of the impurities on the properties of FeSi was investigated theoretically and systematically with the help of FactSage simulations. The impact of three major impurities associated with recycled Si (Al, Cu and Sn) were analysed when present individually and then all together. The analysis was done with the help of phase diagrams for solidification process occurring under equilibrium conditions. It was found that the impurities impact the proportion of the final phases and the melting and phase-transition temperatures. Further, the presence of different intermetallic phases could impact the mechanical properties of the alloy as well. The presence of three impurities together with Fe and Si leads to a complex multicomponent system. While further experiments are needed to identify the actual phases formed during such process, this work provides as framework for carrying out such experiments in the future.

Keywords: Ferrosilicon, recycling, decarbonization, e-waste, FactSage

1. Introduction

Ferrosilicon (FeSi) is produced using a carbothermal process, usually in submerged arc furnaces. Quartzites (SiO_2) are used as the silicon source in the production of FeSi while coke (coal or wood chips) is the primary source of carbon reductant [1,2] . Recycled steel scrap is the primary source of iron (called iron chips) [3]. The iron lowers the partial pressure of silica (SiO_2) required for reduction and forms FeSi solutions that reduce the activity of Si. Hence the process could be carried out at lower temperatures that are employed for the production of silicon. This also results in higher Si yield (less of SiO_2) and lower energy consumption per ton of metal [4] . Approximate charge composition, energy demand and silicon yield for ferrosilicon smelting in a closed furnace for each ton of FeSi produced is shown in Table1 [4] .

The carbothermic reduction of the silicon process releases huge amounts of greenhouse gases, leading to energy losses. It has been estimated that unto 3.4 t of CO_2 can be released per tonne of FeSi produced [4]. To combat climate change, it is imperative to limit the amount of greenhouse gasses emitted during production process. The major source of greenhouse gas emissions during the production of FeSi is the carbothermic reduction of SiO_2. If an alternate source of Si is used, where the silicon not available in its

oxide form, it would be possible to eliminate the use of carbon, thus preventing the greenhouse gas emissions.

Silicon recovered from electronic waste such as photovoltaic panels and waste electronic equipment could provide silicon in its elemental form. Recycling the metal-contaminated silicon destined for landfills for manufacturing FeSi, using only electricity as the source of energy could potentially lead to a reduced carbon footprint. In recent years, there has been growing interest in the use of recycled material for the production of ferrosilicon [5–11]. Recently the use of silicon from photovoltaic (PV) panels along with waste from aluminium refinery was suggested as raw material sources for the production of FeSi [12]. The electronic waste is usually crushed and subjected to a primary separation process, where large pieces of metals, plastic, glass etc are separated efficiently[13] . The recycled silicon recovered from e-waste such as PV panels can has several other metal impurities in small quantities such as aluminium (Al), copper (Cu) and tin (Sn), as these metals are used to make electrical contacts in PV panels and other electronic devices [14,15]. It should be noted that the copper and aluminium used for external wires and mechanical frames respectively, are easily recovered and recycled [16]. Small number of materials that are used directly on silicon for making metal contacts are difficult to separate, without use of expensive and often hazardous chemical processes [12,14,17]. An estimated distribution of different materials associated with Si recovered from electronic waste is given in table 2, along with the relative ease of recovery and qualitative economic value. In the context of this work, the ease of recovery is identified to be 'difficult' if the material to be recovered is alloyed with two or more materials, and separation, recovery and purification involves more than two different materials/components/chemicals. The ease of the recovery process is identified as 'medium', if target material is in unalloyed state and/or maximum two materials/components are involved in its extraction, separation and purification. The process is identified as 'simple', if the material is in unalloyed state and only one material/process is involved in its separation and recovery.

Although silver is also used, especially in PV panels to make contacts, it can be separated from the silicon using simple chemical leaching processes [13,14,17]. However, the remaining metals are neither easy nor commercially attractive to recover, making the process commercially non-viable [14,15]. While the metal-contaminated silicon is unsuitable for the electrical or PV industry, as it requires Si of extremely high purity, it can be used in the metallurgical industry as a silicon source for producing FeSi. There are several uses of FeSi in the metallurgy industry. It is used as a deoxidizer, as a silicon carrier to produce alloys such as silicon steel and other alloying agents' carrier. The composition of the FeSi plays a crucial role in determining the quality of the final product [4]. Therefore, it would be helpful to understand the role of the impurities in the FeSi manufacturing process and the impact on the final availability of the Si for the desired process.

The Fe-Si-Al system have been investigated to some extend both theoretically and experimentally [18–21]. Researchers have analysed the thermodynamics of FeSiAl alloy systema and have tried to synthesise the intermetallic compounds formed in such system [18,19,22]. In some cases, Fe-Si-Al alloys have also been investigated for their magnetic properties and applications in foundry industries [23–27]. Similarly, inclusion of Cu in FeSi systems have been investigated by researchers understand the intermetallic formation and their precipitation behaviour[28,29]. In some cases, a metastable liquid phase separation was investigated, where more than one melt separation took place in FeSiCu undercooled alloys under appropriate conditions[30,31]. Effect of addition of Cu to the properties of Ferritic steel and in alloys for thermoelectric applications have also been investigated [32,33]. Similarly, Fe-Si-Sn system have also been investigated by researchers both theoretically and experimentally [34,35]. In one study, the effect of addition of Sn to the sintering process of 6.5% Si-steel was also experimentally investigated [36]. All these published works show increased interest in the investigation of such inclusions in the FeSi and other ferrous and nonferrous metallurgical applications. However, systematic understanding of such multicomponent phase systems with regards to the different components formed and the cooling behaviour have not been sufficiently investigated in the published literature. The impact of a complex multicomponent system when all such impurities are present simultaneously is also missing in the published literature.

In this work, theoretical investigations of the impact of the metal contaminants in the recycled Si recovered from electronic waste on the phases formed during the production of FeSi were performed. The FeSi alloys with different impurities are considered. The impact of the impurities on the solidification of the alloys is simulated and analyzed with the help of calculated phase diagrams. All the analysis presented in this work are performed for the conditions of equilibrium solidification, which is considered as a benchmark for the real solidification process. The equilibrium solidification is assumed to take place when the rate of solidification is infinitesimally small [37]. Three major metallic impurities, Al, Cu and Sn are considered in different weight percentages. The number and amount of the final phases expected to be formed along with other physical properties such as the onset of solidification, the number and types of phase transitions and the complete solidification temperature are compared. With the help of the simulated data, inferences are drawn related to the suitability of using Si recovered from electronic waste as Si source in the production of FeSi.

Table 1.
Typical Materials and Energy Demand for Smelting of FeSi in Closed Furnaces (for 1 ton of alloy) [4]

FeSi Alloy	FeSi20	FeSi25	FeSi45	FeSi65	FeSi75
Quartzite, kg	370	552	931	1568	1930
Iron chips, kg	810	780	658	343	250
Coke, kg	200	280	438	720	845
Electrode paste, kg	8	10	16	43.3	54
Electricity, MWh/t	2.1	2.7	4.8	7.4	8.8
Silicon yield, %	94–95	97–98.5	98–99	92–94	91–93

Table 2.
Material distribution by weight in Si recovered from e-waste after the primary separation process, along with the relative ease in recovering the pure form of the material and the relative economic value [15,38–42] . In the context of this work, the ease of recovery is identified to be 'difficult' if the material to be recovered is alloyed with two or more materials, and separation, recovery and purification involves more than two different materials/components/chemicals. The ease of the recovery process is identified as 'medium', if target material is in unalloyed state and/or maximum two materials/components are involved in its extraction, separation and purification. The process is identified as 'simple', if the material is in unalloyed state and only one material/process is involved in its separation and recovery.

Material (pure)	Weight % [%]	Ease of recovery	Economic value [USD/t]
Silicon	75-98	Difficult	3,000-7,000 [23]
Silver	0.05 – 0.1	Medium	950,000 – 960,000 [23]
Aluminium	2 - 20	Difficult	2,200-2,700 [23]
Copper	2 - 20	Difficult	9,000-10,000 [22]
Tin	1 - 5	Difficult	28,000-29,000 [18]

2. Materials and Research Methodology

In this work the impact of the major impurities found in recycled silicon on the production of FeSi is investigated theoretically. Two types of FeSi alloys are simulated with the help of FactSage 8.3., FeSi45 with 45 wt.% of Si and FeSi75 with 75 wt. % of Si. The formation of FeSi under equilibrium conditions is investigated with the help of FACTSAGE 8.3 software for different impurities present in varying quantities. Several alloy systems are studied. The alloys are first simulated using only a single metal contaminant as the impurity. Later, alloys with multiple impurities present simultaneously are simulated. Here two assumptions have been considered - a) the plastic and other non-metallic components have been removed by simple physical processes [43,44], and b) the scrap steel has extremely low carbon content (<0.2%) and was treated like solvent. Therefore, carbon is not included as a component in the analysis. The percentages of metal mixed with silicon in e-waste were used as the basis of design of hypothetical systems. The mass of Fe and Si was kept constant for one FeSi alloy system, and the impurities were considered as additions. The impurities were considered as percent of added Si, since recycled Si is considered here the main source of impurity.

Five databases were used in the FactSage calculations. The steel database (FSteel), ultra-pure silicon database (Fsupsi), pure substances database (FactPS), Oxide database (FToxid) and miscellaneous compounds database (FTmisc). Each alloy was simulated from a starting temperature of 1500 ℃ until the final temperature of 50 ℃ with calculations performed at temperature steps of 50℃. These calculations were done using the equilibrium module of the FactSage software. All pure solid phases were considered to be included in the simulation. Pure liquids phases were excluded as all alloys were considered as solutions. All intermediate transitions were considered during the calculations. The molar volumes of the solids and liquids were assumed to be negligible. All the calculations were done at a constant pressure of 1 atm.

In this work, we have first studied each impurity in FeSi45 and FeSi75 systems individually, and, later when all the impurities are present simultaneously.

The composition of the FeSi45 and FeSi75 alloys considered for the simulation of FeSi45 and FeSi75 alloy system has been given in Table 3.

Table 3.
Alloy system of FeSi45 and FeSi75 for simulation, showing the individual composition of the alloy without any impurities.

Alloy system	Fe (g)	Si (g)	Total (g)	Si/Fe
FeSi45	55	45	100	0.82
FeSi75	25	75	100	3.00

The details of the FeSi-Al alloys, systems considered in this work, assuming Al to be the only impurity are shown in table 4. The Al added to the system is associated with Silicon, hence it is represented as a fraction of the silicon mass as 5%, 10%, 15% and 20%. For FeSi45, the masses of Fe and Si are kept constant at 55g and 45g respectively, hence the mass of Al and the total mass of the alloy system varies depending on the percentage of Al present in the Si as impurity.

Table 4.
Alloy systems of FeSi45 and FeSi75 with Al as impurity for simulation. The amount of Al expressed as the percentage of silicon varies from 5-20 %

Alloy System	Fe (g)	Si (g)	Al (g)	Total (g)	Al/Si (%)
FeSi45Al5	55	45	2.3	102.3	5
FeSi45Al10	55	45	4.5	104.5	10
FeSi45Al15	55	45	6.8	106.8	15
FeSi45Al20	55	45	9	109	20
FeSi75Al5	25	75	3.8	103.8	5
FeSi75Al10	25	75	7.5	107.5	10
FeSi75Al15	25	75	11.3	111.3	15
FeSi75Al20	25	75	15	115	20

The assumed compositions for investigating the ferrosilicon-copper alloy systems, considering Cu to be the only impurity are presented in Table 5. The Cu added to the system is associated with Silicon, hence, like Al, it is represented as a fraction of the silicon mass as 5%, 10%, 15% and 20%. For FeSi45, the masses of Fe and Si are kept constant at 55g and 45g respectively, hence the mass of Cu and the total mass of the alloy system varies depending on the percentage of Cu present in the Si as impurity.

Table 5.
Alloy systems of FeSi45 and FeSi75 with Cu as impurity for simulation. The amount of Cu expressed as the percentage of silicon varies from 5-20 %

Alloy System	Fe (g)	Si (g)	Al (g)	Total (g)	Al/Si (%)
FeSi45Cu5	55	45	2.3	102.3	5
FeSi45Cu10	55	45	4.5	104.5	10
FeSi45Cu15	55	45	6.8	106.8	15
FeSi45Cu20	55	45	9	109	20
FeSi75Cu5	25	75	3.8	103.8	5
FeSi75Cu10	25	75	7.5	107.5	10
FeSi75Cu15	25	75	11.3	111.3	15
FeSi75Cu20	25	75	15	115	20

The different FeSi45Sn and FeSi75Sn alloy systems studied in this work are listed in Table 6. Here, Sn is considered to be the only impurity present in the ferroalloy system. Sn is usually associated with Silicon, in lower quantities. In this work, the amount of Sn is represented as a fraction of the silicon mass as 1%, 2% and 5%. Similar to other systems, the mass of the masses of Fe and Si are kept constant, while the total mass of the alloy system varies depending on the percentage of Sn present in the Si as impurity.

Table 6.
Alloy systems of FeSi45 and FeSi75 with Sn as impurity for simulation. The amount of Sn expressed as the percentage of silicon varies from 1-5 %

Alloy System	Fe (g)	Si(g)	Sn (g)	Total (g)	Sn/Si (%)	Alloy System
FeSi45Sn1	55	45	0.5	100.5	1	FeSi45Sn1
FeSi45Sn2	55	45	0.9	100.9	2	FeSi45Sn2
FeSi45Sn5	55	45	2.3	102.3	5	FeSi45Sn5
FeSi75Sn1	25	75	0.8	100.8	1	FeSi75Sn1
FeSi75Sn2	25	75	1.5	101.5	2	FeSi75Sn2

In practical applications, the recycled silicon is expected to contain all three major impurities – Al, Cu and Sn. The source of recycled silicon would be the determining factor for the composition of the impurities. If the Si is recovered from the waste PV panels, Al is expected to be the dominant impurity (≈ 20%), while copper and Sn would be in moderate quantities [43]. On the other hand, if Si is recovered from the microprocessors (computers, mobile phones, other electronic devices), Cu (≈10-15% wt.) and Sn (≈ 3-5% wt.) are expected to be present in higher quantities while Al will be present in lower quantities (2-7%wt.) [39,41]. Therefore, two different sources of Si are considered, Al-rich Silicon and Cu rich silicon. Table 7 shows the composition of the different allots considered for the simulation of the alloy systems.

Table 7.
Alloy systems of FeSi45 and FeSi75 with multiple impurities for simulation. The impurities are expressed as the percentage of silicon

Alloy System	Fe (g)	Si (g)	Al (g)	Cu (g)	Sn (g)	Al/Si [%]	Cu/Si [%]	Sn/Si [%]
FeSi45Al20Cu10Sn2	55	45	9	4.5	0.9	20	10	2
FeSi75Al20Cu10Sn2	25	75	15	7.5	1.5	20	10	2
FeSi45Al5Cu10Sn5	55	45	2.3	4.5	2.3	5	10	5
FeSi75Al5Cu10Sn5	25	75	3.8	7.5	3.8	5	10	5

3. Results and Discussions

3.1. FeSi45 and FeSi75 systems

It is helpful to begin the discussion with the general FeSi45 and FeSi75 systems and present a general overview of the phases and transformations during cooling. This discussion forms the basis to develop further discussions and analyses of the alloy systems with impurities. FeSi systems have been thoroughly studied in the past [4,45–48]. The composition of the alloy considered for the simulation of FeSi45 and FeSi75 alloy system has been given in Table 3. A snapshot of the salient features of the FeSi45 and FeSi75 alloy systems, as analysed with the help of FactSage simulations is given in Table 8.

Table 8.
Characteristics of FeSi45 and FeSi75 alloys obtained from FactSage simulations

Alloy System	Onset of solidification (Tos) (°C)	Completion of (Tcs) solidification (°C)	Intermediate phases	Final phases (fraction % wt)
FeSi45	1295	1210	Fe3Si7	FeSi (30.9), FeSi2 (69.1)
FeSi75	1300	1213	Fe3Si7	Si_A4 (49.9), FeSi2 (50.1)

The corresponding binary phase diagram for the system with silicon concentration (wt.%) expressed as the fraction of the total mass of Fe and Si is shown in Figure 1. Only a portion of the entire phase diagram is shown with Si/(Fe+Si) ranging from 0.4 to 0.8. The Diamond-A4 phase appearing for alloys with more than 57% Si (wt%) is a silicon solid solution dissolving limited amounts of Fe, P, C and Sn. For the FeSi75 alloys considered in this work, the Si diamond-A4 phase, which makes up ≈ 49.9% of the alloy,

dissolves 2.1x10^{-28} g of Fe. Despite the differences in the Si concentration, both alloys begin and end the process of solidification around similar temperatures and both systems have one intermediate phase (Fe_3Si_7). The Fe_3Si_7 phase begins to form at ≈1210.6 ℃ for FeSi45 and ≈1213.6 ℃ for FeSi75. The intermediate Fe_3Si_7 phase is stable up to ≈ 995.8 ℃ in FeSi45 below which it undergoes solid state phase transformation to $FeSi_2$. In the case of FeSi75, the presence of the Si-diamond phase stabilizes the intermediate Fe_3Si_7 phase to a lower temperature of ≈ 947.8 ℃. As the alloys cool below this temperature, the Fe_3Si_7 phase undergoes the phase transition to $FeSi_2$. During the cooling, the proportion of the intermediate Fe_3Si_7 phase remains practically constant for both FeSi45 and FeSi75 and under equilibrium conditions, the entire amount converts into the stable $FeSi_2$ phase.

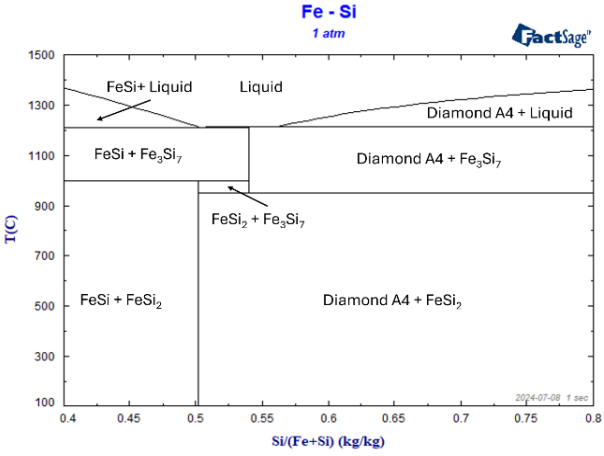

Fig. 1. Fe-Si binary phase system diagram. X axis represents Si/(Fe+Si). Figure produced with the help of FactSage

3.2. FeSi45 and FeSi75 with Al as impurity

Al is among the most common impurity in the FeSi alloys. Commercially produced ferrosilicon usually contains between 0.5-2% if Al as impurity [4,49]. However, since Al is used as an electrical contact in most electronic devices, due to its excellent electrical conductivity, less weight and not easily diffusing into Silicon below 300 ℃ [50–52]. Table 9 shows the important characteristics of FeSi45Al5-20, and FeSi75Al5-20 alloys based on the simulations done in FactSage.

3.2.1. FeSi45Al5-20 alloy systems

Figure 2 shows the phase diagrams of FeSi45Al5-20 alloy system. In this diagram, the ratio of Si/Fe is kept constant (0.82 = 45/55) for FeSi45 and the ratio of Al to Si is varied from 0 to 0.25 (0 – 25%). The fraction of the total alloy mass contributed by the final phases in the different FeSi45Al alloys is shown in Fig 3.
When the Fe/Si ratio is kept fixed at 0.82 (45/55), i.e. the temperature at which the alloy is expected to begin to solidify (T_{os}) reduces with the increase in the percentage of Al. The T_{os} reduces from 1274℃ for 5% wt. of Al to 1226℃ for 20% wt. of Al. Since this is accompanied by the lower value of total free energy change (ΔG) at the beginning of solidification, and since FeSi is the only phase to precipitate, we speculate that addition of Al increases the critical radius of the crystallization. As the content of Al in the alloy increases, a larger crystallite is probably required to sustain the grain growth and solidification, which in turn would result in lower solidification temperatures. In all cases, FeSi is expected to be the first phase to solidify. The amount of FeSi initially precipitated from the alloy decreases with the increase in Al content. For example, at 1200 ℃, the FeSi formed in FeSi45Al20 is only 43% of the FeSi formed in FeSi45Al5. The completion of the solidification for the FeSi45Al5-20 alloy systems was also found to depend on the content of Al in the alloy. The alloys, with 5-10% wt. of Al, are expected to completely solidify at 899℃ while the alloys with 15-20% wt. Al became completely solid at 893℃. The alloys also show a difference in the cooling behaviour and the intermediate phases formed depending on the Al content.

Table 9.
Temperature of onset of solidification (T_{os}), the temperature of completion of solidification (T_{cs}), the intermediate phases formed and the final phases for different FeSiAl alloy systems simulated using FactSage under equilibrium cooling conditions.

Alloy System	Alloy sub-system	Onset of solidification (T_{os}) (℃)	Completion of solidification (T_{cs}) (℃)	Intermediate phases	Final phases
FeSi45	FeSi45Al5	1274	899	Fe_3Si_7, Fe_2SiAl_2, $FeSiAl_2$	FeSi, $FeSi_2$, $Al_5Fe_2Si_2$
	FeSi45Al10	1256			
	FeSi45Al15	1240	893		
	FeSi45Al20	1226			
FeSi75	FeSi75Al5	1319	840	Fe_3Si_7	Si_A4 (diamond), $FeSi_2$, Al_3FeSi_2
	FeSi75Al10	1296			
	FeSi75Al15	1273			
	FeSi75Al20	1253			

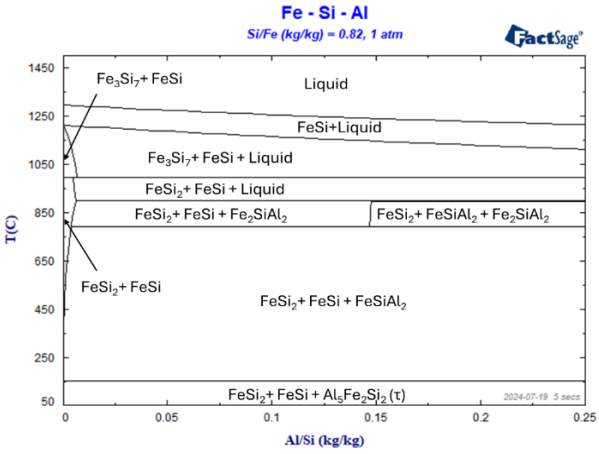

Fig. 2. Phase diagram of FeSi45 alloy systems with Al as impurity. The quantity of aluminium in the alloy systems varies as a percentage of Si from 5-20%. In this phase diagrams, the ratio Si/Fe is held constant (45/55 = 0.82) while the ratio Al/Si is varied from 0-0.25

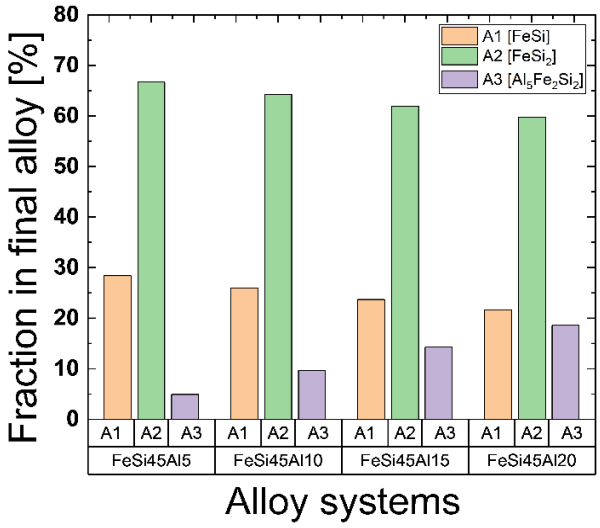

Fig. 3. Fraction of the total mass of the different FeSi45Al alloy systems contributed by the individual stable phases at 50 °C presented as percent of the total mass. For the sake of clarity in the image, the final phases have been replaced by respective symbols in the image; FeSi (A1), $FeSi_2$ (A2) and $Al_5Fe_2Si_2$ (A3)

In FeSi45 alloys, which have Al content ranging from 1.5 to 14.9%wt, FeSi is present throughout the cooling and solidification process. The amount of FeSi phase increases in quantity initially, where more FeSi crystallize out of the liquid solution. Fe_3Si_7 is the second phase to be formed as the cooling progresses. The amount of FeSi in the alloy increases until the transformation of the Fe_3Si_7 phase, which is only stable at higher temperatures accompanied by the appearance of $FeSi_2$ phase. The last portion of the liquid first solidifies into Fe_2SiAl_2 phase which soon undergoes a solid phase transition to $FeSiAl_2$ phase. The increase in the quantity of $FeSi_2$ phase and the corresponding decrease in the quantity of FeSi phase continues until the appearance of $FeSiAl_2$ phase. At higher temperatures, both the Fe_3Si_7 and $FeSi_2$ phases contains Al in the in the form of Fe_3Al_7 and $FeAl_2$ respectively. However, as temperature reduces, Al precipitates out of the mixture leading to the increased proportion of stable $FeSi_2$ phase. For example, just before the $Fe_3Si_7 \leftrightarrow FeSi_2$ phase change, the Fe_3Si_7 phase could contain ≈0.98% wt. Fe_3Al_7. Similarly, immediately after the transition to $FeSi_2$ under equilibrium conditions, the $FeSi_2$ phase may contain ≈0.6 % wt. of $FeAl_2$. As cooling proceeds further below 790°C, both FeSi and $FeSiAl_2$ phases increase in amount, while that $FeSi_2$ continues to decrease. The increase in the proportion of $FeSiAl_2$ phase occurs at the expense of Fe (Si, $Al)_2$ phase mixture. Finally, at ≈ 148°C, $FeSiAl_2$ undergoes a solid-state transition to $Al_5Fe_2Si_2$. Under equilibrium conditions, the proportion of $FeSi_2$ decreases on cooling, while those of FeSi and $Al_5Fe_2Si_2$ keeps increasing. At 50°C, the $FeSi_2$ phase is expected to contain ≈ $1x10^{-10}$ % of $FeAl_2$ phase by weight. The fraction of each individual phase at 50°C is shown in Fig 3.

FeSi45 alloys systems with Al content greater than 15% wt., undergo slightly different transition and encounter different phases as they cool down. They differ from the FeSi alloys containing Al<15%, in two major ways. First, the temporary disappearance of FeSi phase during cooling, and second the co-existence of Fe_2SiAl_2 and $FeSiAl_2$ phases during the cooling. As the alloys cools down, the first phase to crystalize is still the FeSi phase, which increases in proportion until the $Fe_3Si_7 \leftrightarrow FeSi_2$ phase change reaction occurs under equilibrium conditions at ≈ 992.9 °C. As cooling proceeds, the proportion of FeSi phase reduces continuously until ≈ 899°C, where the entire remaining FeSi phase disappears, and the Fe_2SiAl_2 phase appears, accompanied by marked increase in the proportion of $FeSi_2$ phase. As the alloys cools further, the $FeSiAl_2$ phase appears at 893°C, when the entire alloy is in solid state. As the alloy cools down further, at ≈789°C the Fe_2SiAl_2 transforms to $FeSiAl_2$, accompanied by the reappearance of FeSi phase and the corresponding decrease in the proportion of $FeSi_2$ phase. The FeSi phase remains stable hereafter, steadily increasing in proportion until 50°C. The transition of $FeSiAl_2$ to $Al_5Fe_2Si_2$ remains same as in the alloys with lower Al content.

In FESi45Alx (5≤x≤20) alloy systems, the final alloy is dominated by the proportion of $FeSi_2$ phase, which constitutes >60% of the alloy for all cases investigated, even when Al is 20% of the added Si. The FeSi phase appears as the second major constituent of the alloy systems, ranging between 30% - 20% of the total alloy mass, decreasing proportion with the increasing Al content. $Al_5Fe_2Si_2$ phase comprises the remaining portion of the alloy, its mass increasing to just below 20% of the total alloy mass for FeSi45Al20 alloy.

3.2.2. FeSi75Al5-20 alloy systems

Figure 4 shows the phase diagrams of FeSi75Al5-20 alloy system. In this diagram, the ratio of Si/Fe is kept constant (3=75/25) for FeSi75 and the ratio of Al to Si is varied from 0 to 0.25 (0 – 25%). The fraction of the total alloy mass contributed by the final phases in the different FeSi75Al alloys is shown in Fig 5. In FeSi75 alloys, the ratio Si/Fe is fixed at 3, but in reality, the ratio could be slightly above or below 3. The aluminium added to FeSi75 is considered associated with the Si and is expressed as a percentage of silicon, ranging from 5-20%. As can be seen from Table 9 and Fig 4, the temperature at which the solidification begins decreases continuously with an increasing percentage of Al

in the alloy system. For FeSi75Al5, the first solid crystals of Si-A4 appear at ≈ 1319°C, while the crystallization begins at ≈1253°C for FeSi75Al20. However, unlike in FeSi45 alloy systems, the Al content has no impact on the completion of solidification temperature and all alloy systems exist as complete solid phases below 840 °C. Interestingly, although the onset of solidification temperature for FeSi75Alx (5≤x≤20) alloys is higher than the corresponding FeSi45Alx alloys, the temperature at which the solidification is complete is lower than all the FeSi45Alx alloys considered in this work. This means the FeSi75Alx alloys contain a liquid phase for a longer duration than the FeSi45Alx alloys.

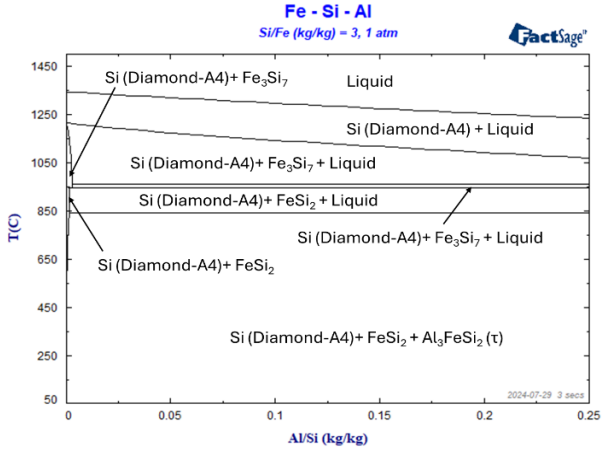

Fig. 4. Phase diagram of FeSi75 alloy systems with Al as impurity. The quantity of aluminium in the systems varies as a percentage of Si from 5-20%. In this phase diagrams, the ratio Si/Fe is held constant (75/25 = 3) while the ratio Al/Si is varied from 0-0.25

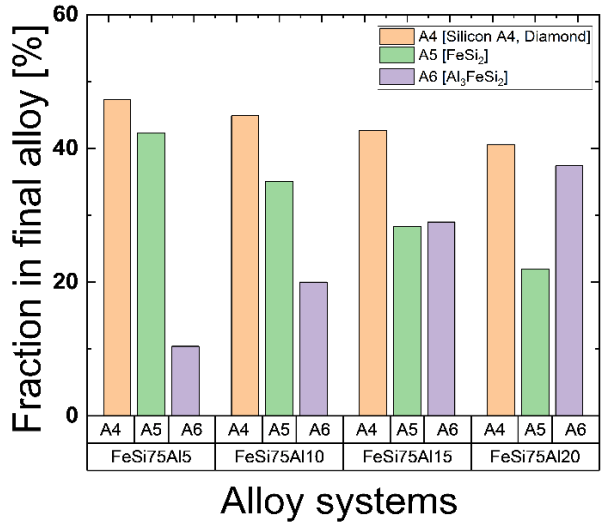

Fig. 5. Fraction of the total mass of the different FeSi75Al alloy system contributed by the individual stable phases at 50 °C presented as percent of the total mass. For the sake of clarity in the image, the final phases have been replaced by respective symbols in the image; Silicon-A4-diamond (A4), $FeSi_2$ (A5) and Al_3FeSi_2 (A6)

As the FeSi75Alx alloys cool down, the Si-diamond phase is the first phase to crystallise. The Si diamond phase is actually a solid solution dissolving limited amount of Al and Fe. The amount of Al in the initially solidified Si -A4 crystals increases with a commensurate decrease in the amount of Fe as the percentage of Al in the alloy increases. In the FeSi75Al5 alloys, the wt. fractions of Al and Fe at 1200 °C are 1.5 $x10^{-5}$ and 2.7 $x10^{-7}$ respectively. The corresponding values change to 1.7 $x10^{-5}$ (Al) and 1.6 $x10^{-7}$ (Fe) for FeSi75Al20 alloy. As the liquid alloy cools, the Si from the liquid continues to precipitate as Si-A4 while the amount of Fe and Al in the liquid phase remains almost constant. The Fe_3Si_7 begins to precipitate from the liquid as an intermediate phase at temperatures between 1173 °C (for FeSi75Al5) and 1091 °C (for FeSi75Al20). As cooling progresses, at ≈960°C, the liquid, which was silicon rich to begin with, now has almost equal masses of Si and Al and the amount of Fe in the liquid is nearly half that of both. At ≈ 942°C, Fe_3Si_7 phase transforms to $FeSi_2$ phase. A cooling progresses, the liquid solution increasingly becomes richer in Al, as more Si-A4 and $FeSi_2$ phases precipitate. Finally, at ≈ 840°C, the remaining liquid solidifies into Al_3FeSi_2. Both FeSi and $FeSiAl_2$ do not appear in FeSi75Alx alloys systems. Increase in the amount of Si in FeSi, stabilizes the Al_3FeSi_2 and promotes its formation at higher temperature. In FeSi45Alx systems, the $Al_5Fe_2Si_2$ formed only at temperatures below 150 °C, while in FeSi75Alx systems the Al_3FeSi_2 is formed at 840 °C. In FeSi75Alx systems, the proportion of Al_3FeSi_2 phase increases with the increasing content of Al, and for FeSi75Al15 and FeSi75Al20, the Al_3FeSi_2 is the second most available phase next to Si-A4 phase (Fig 5). This is understandable due to the increased amount of Si in FeSi75 systems, the impurities associated with the Si would also increase commensurately.

3.3. FeSi45 and FeSi75 with Cu as impurity

Copper is generally used in most electrical circuits and equipment due to its excellent electrical conductivity and lower cost than silver [53]. Therefore, copper is widely used in electronic applications[54,55], although it may not be used directly on silicon to form electrical contacts [56,57]. Copper diffuses readily in silicon owing to its small ionic radius and weak interaction with Si lattice. This makes copper highly diffusive even at room temperatures and impacts the stability of copper complexes in silicon [58,59]. Copper may also enter as a contaminant during primary processing of silicon, such as during wafering stage using wire saw [60]. Copper may be present in silicon as impurity ranging from extremely minute quantities up to 20% by weight [40–42,61]. The extraction of copper from silicon is rather complicated due to the high diffusivity of copper in silicon[40,42,61]. Hence, copper is more likely to be associated with silicon recovered from electronic waste.

Table 10 shows the characteristics of FeSi45Cu and FeSi75Cu alloy systems based on the FactSage simulations. Figures 6 and 8 show the phase diagrams of FeSi45Cu and FeSi75Cu systems respectively. In these diagrams, the ratio of Si/Fe is kept constant (0.82 (45/55) for FeSi45 and 3 (75/25) for FeSi75) and the ratio of Cu to Si is varied from 0 to 0.25 (0 – 25%). The fraction of the total alloy mass contributed by the final phases in the different FeSi45Cu alloys are shown in Fig 7 while the same for FeSi75Cu alloys are shown in Fig 9.

Table 10.
Temperature of onset of solidification (T_{os}), the temperature of completion of solidification (T_{cs}), the intermediate phases formed and the final phases for different FeSiCu alloy systems simulated using FactSage under equilibrium cooling conditions.

Alloy System	Alloy sub-system	Onset of solidification (T_{os}) (°C)	Completion of solidification (T_{cs}) (°C)	Intermediate phases	Final phases
FeSi45	FeSi45Cu5 FeSi45Cu10 FeSi45Cu15 FeSi45Cu20	1293 1292 1291 1291	839	Fe_3Si_7, $Cu_{19}Si_6$	FeSi, $FeSi_2$, $Cu_{15}Si_4$
FeSi75	FeSi75Cu5 FeSi75Cu10 FeSi75Cu15 FeSi75Cu20	1328 1313 1299 1284	801	Fe_3Si_7	Si_A4 (diamond), $FeSi_2$, $Cu_{19}Si_6$

3.3.1. FeSi45Cu5-20 alloy systems

Fig 6 shows the phase diagram for phase diagrams of FeSi45Cu system. The fraction of the total alloy mass contributed by the final phases in the different FeSi45Cu alloys are shown in Fig 7.

For FeSi45 alloys, with Cu as an impurity, the temperature above which the entire alloy exists as liquid does not change considerably with the addition of Cu, for the alloys analysed in this work. As seen in Fig 6, FeSi45 alloys containing 5%wt. Cu, the alloy begins to solidify at 1293 °C, while those containing 20% wt. Cu, the solidification begins at 1291 °C, which is only a difference of 2°C. All the alloys, regardless of the Cu content completely solidify at the same temperature of 839 °C. For all FeSi45 alloys with Cu, FeSi is the first phase to solidify. The amount of copper in the FeSi45 alloy has a greater impact on the precipitation temperature of intermediate phase Fe_3Si_7, which is the next compound to precipitate from the solution. This is clearly visible in fig 6. For FeSi45Cu5, precipitation of Fe_3Si_7 begins at a temperature of 1200 °C, while in FeSi45Cu20 alloy, its precipitation does not occur until 1172 °C. As cooling proceeds, Fe and Si continue to precipitate from the solution with corresponding increase in the amount of FeSi and Fe_3Si_7.

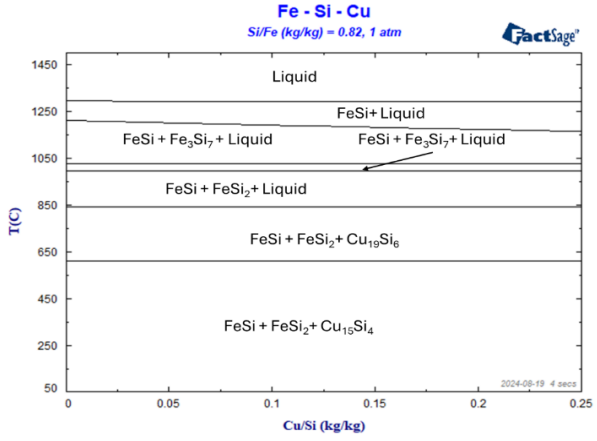

Fig. 6. Phase diagram of FeSi45 alloy systems with Cu as an impurity. The quantity of copper in the alloy systems varies as a percentage of Si from 5-20%. In this phase diagrams, the ratio Si/Fe is held constant (45/55 = 0.82) while the ratio Cu/Si is varied from 0-0.25

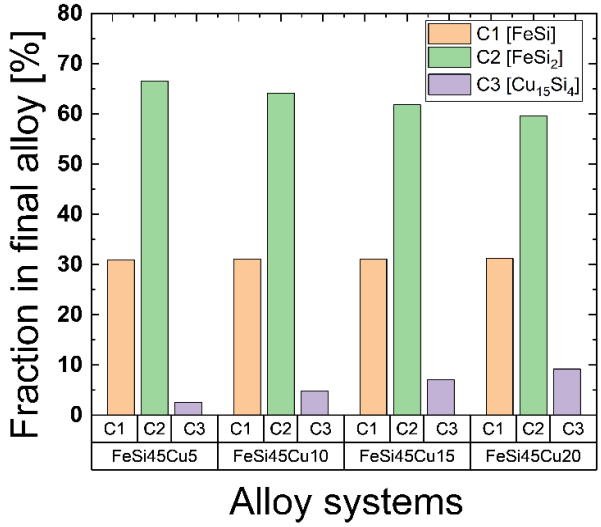

Fig. 7. Fraction of the total mass of the different FeSi45Cu alloy systems contributed by the individual stable phases at 50 °C presented as percent of the total mass. For the sake of clarity in the image, the final phases have been replaced by respective symbols in the image; FeSi (C1), $FeSi_2$ (C2) and $Cu_{15}Si_4$ (C3)

At ≈1024°C, the liquid solution contains primarily Cu and Si, with almost all Fe precipitated out as FeSi and Fe_3Si_7. This is understandable as studies have earlier reported the low solubility of Cu and Fe, especially at lower temperatures[62,63]. At ≈ 995 °C, Fe_3Si_7 undergoes a solid-state transition to $FeSi_2$ which is a stable phase and forms the largest component of the alloy by mass (Fig 8). Finally, at ≈ 839 °C, the remaining copper rich solution solidifies to $Cu_{19}Si_6$ which, in this case is an intermediate phase and stable only at higher temperatures. Here it can be seen that addition of Si causes the Cu to remain in molten state well below its melting point of 1084 °C. As cooling progresses the system remains stable, and all the components maintain their individual masses. Finally, at ≈ 608 °C, $Cu_{19}Si_6$ transforms to $Cu_{15}Si_4$ which is a stable phase and remains so at room temperature. Below this temperature, no further chemical reactions or changes in the masses of individual component occur as the alloy cools to 50 °C. $FeSi_2$ remains the largest component by mass in the final alloys for all different compositions of FeSi45Cu alloys. As the proportion of Cu

increases in the alloy, the proportion of $FeSi_2$ reduces, with the corresponding increase in the proportion of $Cu_{15}Si_4$. The proportion of FeSi increases minimally with the increase in the proportion of Cu in the alloy. The proportion of masses of the individual component in the different FeSi45Cu alloy systems at 50 ℃ is shown in Fig 7.

3.3.2. FeSi75Cu5-20 alloy systems

Fig 8 shows the phase diagram FeSi75Cu system. The proportion of masses of the individual component in the different FeSi75Cu alloy systems at 50 ℃ is shown in Fig 9.

For FeSi75 alloys, the amount of Cu in the alloy has a more pronounced impact on the onset of solidification temperature as seen from table 10 and Fig 8. The FeSi75Cu5 alloys begin to precipitate Si (Diamond structure) at ≈1328 ℃, while in the FeSi75Cu20 alloys, the precipitation of Si occurs at ≈1284 ℃. This represents a difference of 44 ℃, which is in stark contrast with the behaviour of FeSi45Cux ($5 \leq x \leq 20$) alloys. The Fe_3Si_7 is the next phase to precipitate as the cooling progresses. The precipitation temperature of Fe_3Si_7 is also affected by the proportion of Cu in the alloy, albeit the impact is less pronounced than on the precipitation temperature of Si. In FeSi75Cu5 alloys, the precipitation of Fe_3Si_7 begins at ≈1197 ℃, while it occurs at ≈ 1172 ℃ in FeSi75Cu20 alloys (a difference of 25 ℃). As cooling progresses, most of the Fe precipitates out of the solution, leaving behind a predominantly Cu-Si liquid solution. At ≈ 947 ℃, the Fe_3Si_7 undergoes the solid-state transition to $FeSi_2$. The Fe_3Si_7 to $FeSi_2$ transition occurs at a temperature ≈ 50℃ lower than that in FeSi45Cu alloys. As cooling proceeds, almost all of Fe from the liquid precipitates and the Cu-Si solution solidifies into $Cu_{19}Si_6$ compound at ≈ 801 ℃. In FeSi75Cu alloy systems, the $Cu_{19}Si_6$ remains stable and does not undergo further transition as expected in FeSi45Cu systems. The components and their amounts remain relatively stable as the alloy cools to 50 ℃. In FeSi75Cu alloy systems, both $FeSi_2$ and Si contribute almost equally to the final mass of the alloy as shown in Fig 9. However, as the proportion of copper increases, the proportion of Si in the final alloy reduces more than that of $FeSi_2$.

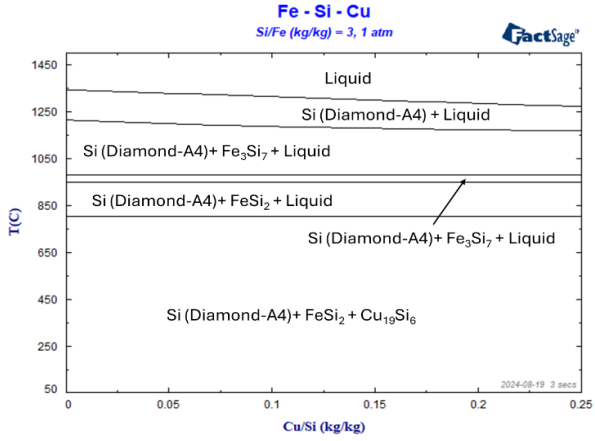

Fig. 8. Phase diagram of FeSi75 alloy systems with Cu as impurity. The quantity of copper in the alloy systems varies as a percentage of Si from 5-20%. In this phase diagrams, the ratio Si/Fe is held constant (75/25 = 3) while the ratio Cu/Si is varied from 0-0.25

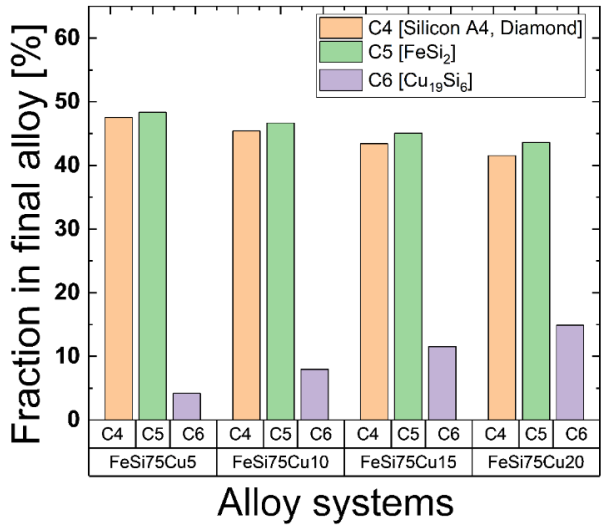

Fig 9: Fraction of the total mass of the different FeSi75Cu alloy systems contributed by the individual stable phases at 50 ℃ presented as percent of the total mass. For the sake of clarity in the image, the final phases have been replaced by respective symbols in the image; Silicon-A4-diamond (C4), $FeSi_2$ (C5) and $Cu_{19}Si_6$ (C6)

3.4. FeSi45 and FeSi75 with Sn as impurity

Sn is used in electronic components usually for soldering purposes. Depending on the number of such soldered contacts in the electronic device, the amount of Sn in the recycled Si waste recovered from electronic waste could be up to 3% by wt. [18,19]. Pure tin has extremely low melting point of 231.9 ℃. Usually, eutectic alloys of tin with lead, indium or zinc are used, which melt at even lower temperatures [18]. Solid solubilities of tin in silicon have been found to be negligible [64], while finite solubility has been reported for Fe-Sn systems [65].

Table 11 shows the characteristics of FeSi45Sn and FeSi75Sn alloy systems based on the FactSage simulations. Figures 10 and 12 show the phase diagrams of FeSi45Sn and FeSi75Sn systems respectively. In these diagrams, the ratio of Si/Fe is kept constant as earlier, and the ratio of Sn to Si is varied from 0 to 0.05 (0 – 5%). The fraction of the total alloy mass contributed by the individual stable phases at 50℃ in the different FeSi45Sn alloys are shown in Fig 11 while the same for FeSi75Sn alloys are shown in Fig 13.

Table 11.
Temperature of onset of solidification (T_{os}), the temperature of completion of solidification (T_{cs}), the intermediate phases formed and the final phases for different FeSiSn alloy systems simulated using FactSage under equilibrium cooling conditions

Alloy System	Alloy sub-system	Onset of solidification (T_{os}) (°C)	Completion of solidification (T_{cs}) (°C)	Intermediate phases	Final phases
FeSi45	FeSi45Sn1 FeSi45Sn2 FeSi45Sn5	1294 1293 1291	232	Fe_3Si_7	FeSi, $FeSi_2$, Sn
FeSi75	FeSi75Sn1 FeSi75Sn2 FeSi75Sn5	1342 1341 1338	232	Fe_3Si_7	Si_A4 (diamond), $FeSi_2$, Sn

3.4.1. FeSi45Sn1-5 alloy systems

The inclusion of Sn alone as impurity in FeSi systems has minimal impact on the final product formed. Although Sn has been reported to have finite solubility in Fe [65], when present together as FeSi, Sn does not form any compounds with Fe and simply precipitates as Sn. In FeSi45Sn systems, with the proportion of Sn varying between 1-5%wt. of Si, the impact on the temperature at which first solid phase appears and the temperature below which the entire alloy is solid does not change significantly. The T_{os} decreases by ≈ 1.67°C / gm Sn. When the Sn content is 5% wt. of Si, the temperature of the onset of solidification is expected to reduce by 3 °C. FeSi45 alloys with 1-5% wt. Sn, exhibit similar cooling behaviour for the entire range of Sn composition considered in this work. At ≈ 1294°C, FeSi is the first phase to crystallize and precipitate out of the liquid. The amount of FeSi precipitated almost doubles between 1250 and 1200 °C under equilibrium cooling. The increase in the amount of FeSi slows as Fe_3Si_7 appears and later the amount of FeSi even reduces as $FeSi_2$ is formed. Fe_3Si_7 is the next compound to form and the temperature of its formation changes marginally with the change in the composition of the alloy. For FeSi45Sn1, Fe_3Si_7 begins to form at ≈1209°C, while for FeSi45Sn5, it is expected to appear at 1205 °C. As cooling progresses, at ≈ 995°C, Fe_3Si_7 transforms to $FeSi_2$, accompanied by an approximately 25% reduction in the amount of FeSi. The transition temperature of Fe_3Si_7 to $FeSi_2$ is not affected by the proportion of Sn in the alloy. At this point almost all of Fe and Si are distributed as solid FeSi and $FeSi_2$ while almost all of Sn remains as liquid. Finally at 231.9 °C, which is the melting point of pure Sn, the liquid Sn solidifies. Since no alloys are formed between Sn and Fe, the proportion of FeSi and $FeSi_2$ in the final alloy do not change with the change in the proportion of Sn.

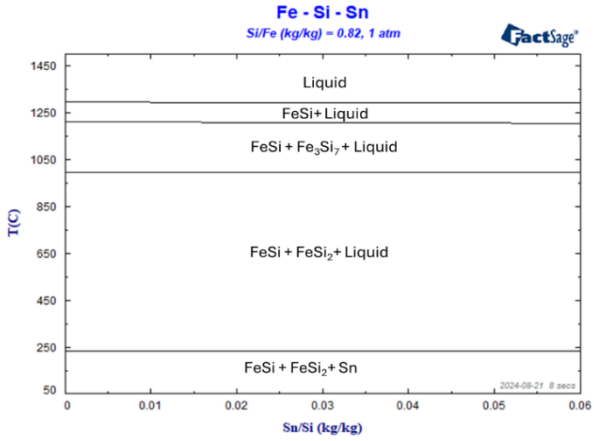

Fig. 10. Phase diagram of FeSi45 alloy systems with Sn as impurity. The quantity of Sn in the alloy systems varies as a percentage of Si from 1-5%. In this phase diagrams, the ratio Si/Fe is held constant (45/55 = 0.82) while the ratio Sn/Si is varied from 0-0.05

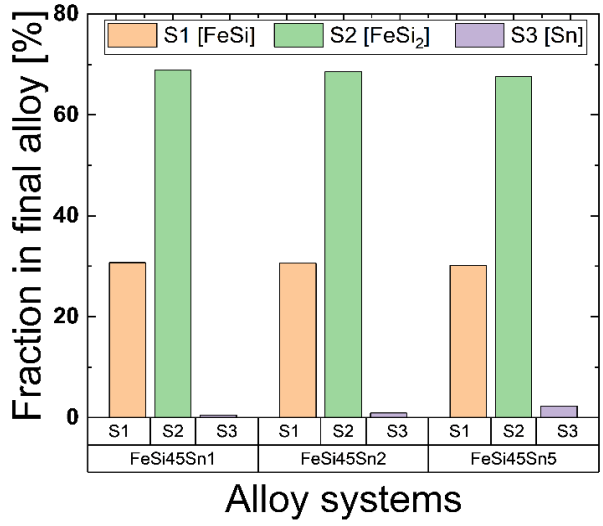

Fig. 11. Fraction of the total mass of the different FeSi45Sn alloy systems contributed by the individual stable phases at 50 °C presented as percent of the total mass. For the sake of clarity in the image, the final phases have been replaced by respective symbols in the image; FeSi (S1), $FeSi_2$ (S2) and Sn (S3)

3.4.2. FeSi75Sn1-5 alloy systems

The FeSi75Sn alloys show slightly similar sensitivity to the presence of Sn as in FeSi45Sn alloy systems, although any changes are imperceptibly smaller. In this case, the T_{os} decreases by ≈ 1.33°C / gm Sn. The proportion of Sn in the alloy changes the temperature at which the Si-Diamond phase begins to crystallize out of the liquid solution as shown in Table 11. The amount of Si precipitated increases continuously until the appearance of Fe_3Si_7 phase.

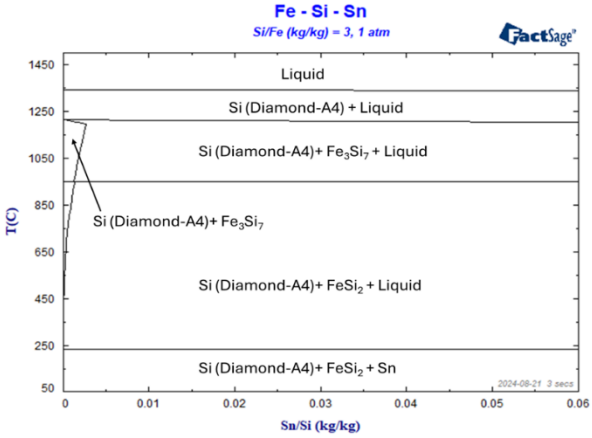

Fig. 12. Phase diagram of FeSi75 alloy systems with Sn as impurity. The quantity of Sn in the alloy systems varies as a percentage of Si from 1-5%. In this phase diagrams, the ratio Si/Fe is held constant (75/25 = 3) while the ratio Sn/Si is varied from 0-0.05

The temperature of appearance of Fe_3Si_7 is slightly reduced with increasing Sn content, from 1209°C at 1%wt Sn to 1205°C for 5% wt. of Sn. As cooling progresses, at 947 °C, the Fe_3Si_7 changes to $FeSi_2$, accompanied by an increase in the amount of Si, as a result of excess Si from Fe_3Si_7 to $FeSi_2$ transition. At this point, the alloy is expected to be composed of almost equal amount of Si and $FeSi_2$ phases, with the Sn remaining as liquid. No further changes occur in the proportion of Si and $FeSi_2$ after the transition of Fe_3Si_7. Finally, at 231.9 °C, the Sn solidifies as pure solid. Hence, in the microstructure of such an alloy, Sn is expected to be distributed among the Si and $FeSi_2$ grains. Since no alloys are formed here as well, the final proportions of Si and $FeSi_2$ do not change with the increase in the proportion of Sn.

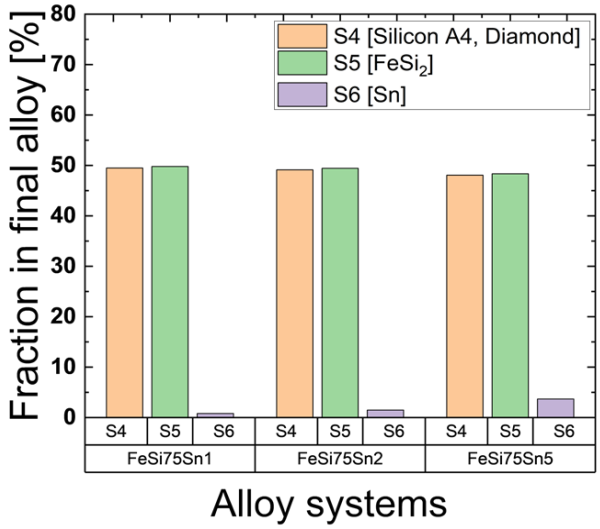

Fig. 13. Fraction of the total mass of the different FeSi75Sn alloy systems contributed by the individual stable phases at 50 °C presented as percent of the total mass. For the sake of clarity in the image, the final phases have been replaced by respective symbols in the image; Si-Diamond (S4), $FeSi_2$ (S5) and Sn (S6)

3.5. FeSi45 and FeSi75 with Al, Cu and Sn present together as impurities

As mentioned earlier, in this section, analysis of FeSi45 and FeSi75 prepared from two sources of recycled silicon are presented i) Al rich recycled Si and ii) Cu rich recycled Si. Table 7 shows the composition of the different allots considered for the simulation of the alloy systems.

3.5.1. FeSi45 alloy made with Al rich recycled silicon

The composition of the alloy systems made from recycled silicon containing Al as the main contamination, along with moderate amounts of Cu and Sn are given in Table 7. For the purpose of this work, the percentages of Al, Cu and Sn in the Si, expressed as a percentage wt. of Si, are considered to be 20%, 10% and 2% respectively. Figure 14 shows the phase diagram created using FactSage for FeSi45Al0-25Cu10Sn2 alloy system. In this phase diagram, the ratios Si/Fe, Cu/Si and Sn/Si were kept constants, and the Al/Si ratio was varied between 0-25% wt. of Si.

Such multicomponent phase diagrams could be extremely complex as seen in Fig 14. Here, we shall attempt to describe only one FeSi45 alloy composition in details (FeSi45Al20Cu10Sn2). Starting at a temperature of 1500°C, the alloy remains as a homogenous liquid phase until ≈1227.8 °C, at which point FeSi begins to precipitate from the solution as the first solid phase. The amounts of molten Al, Cu and Sn are expected to remain stable while those of Fe and Si decrease, as the cooling progresses. At 1112.2 °C, Fe_3Si_7 begins to crystallize. At some lattice points in Fe_3Si_7, Al is expected to replace Si, forming small amounts (<1% wt.) of Fe_3Al_7. As cooling further progresses, the amount of solid FeSi and Fe_3Si_7 continues to increase. At ≈1065°C, the simulation predicts the presence of two immiscible liquid solutions, a Fe-Si

rich solution (Liquid), and an Al-Cu-Sn rich solution (liquid 2). At 1100°C, Fe and Si make up ≈72% (wt.) of Liquid, while Al+Cu+Sn contribute to 88% of the mass of liquid 2. This could probably be due to the difference in the governing equations used for further calculations. Liquid is governed by FS-Steel database while liquid 2 is governed by FS-pure substances database. This further shows the complexity involved in such multicomponent simulations. Beyond 1005.6 °C, only the Al-Cu-Sn rich solution, liquid 2, is expected to exist, dissolving small amounts of Fe and Si as a liquid solution. The Fe-Si rich portion of the solution is expected to solidify completely, contributing to the increase in the masses of FeSi and Fe_3Si_7. The proportion of Fe_3Al_7 in Fe_3Si_7 also increases as temperature decreases, from 0.5% wt. at 1100°C to 0.9% wt. ≈ 993 °C. At this temperature, Fe_3Si_7 transforms to $FeSi_2$. As with Fe_3Si_7, $FeSi_2$ is also expected to have Al at some of its lattice points forming $FeAl_2$. The proportion of $FeAl_2$ in $FeSi_2$ initially increases as the temperature decreases, until 850 °C, after which the Al is expected to diffuse out of the lattice decreasing the proportion of $FeAl_2$. The decrease in the proportion of $FeAl_2$ continues through the cooling period beyond 850 °C until 50 °C (end of simulation). At ≈871°C, the third solid compound, Fe_2SiAl_2 begins to precipitate out of the Al-rich liquid solution. As cooling progresses, more Fe_2SiAl_2 precipitates out of the solution making the solution copper rich. However, the presence of Sn appears to stabilize Cu in liquid state and the $Cu_{19}Si_6$ alloy that was formed in FeSi45Cu alloy systems, does not appear in this alloy system. Despite Al having a lower melting point than copper, the $FeSiAl_2$ alloy precipitates first. At ≈789 °C, Fe_2SiAl_2 transforms to $FeSiAl_2$. As cooling progresses, at ≈ 685°C, a BCC solid solution comprising Cu-Sn-Al and minute quantities of Fe and Si begins to crystallize. Finally, at ≈678.9 °C, the remaining liquid solidifies into a BCC solid solution containing the entire mass of Cu and Sn and ≈ 15% mass of Al, along with minute quantities of Fe and Si.

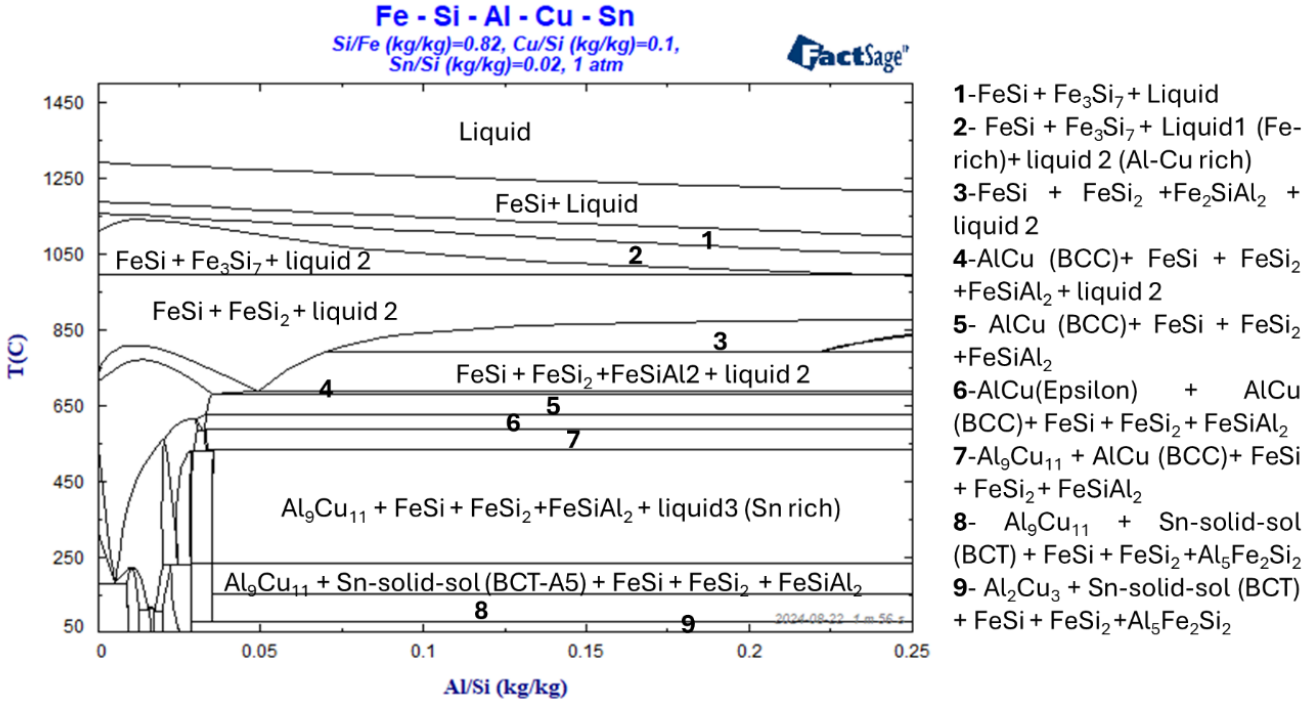

Fig. 14. Phase diagram of FeSi45Al20Cu10Sn2 alloy systems with Al (0-25% wt. of Si), Cu (10% wt. of Si) and Sn (2% wt. of Si) as impurities. In this phase diagram, the ratios Si/Fe, Cu/Si and Sn/Si are kept constants, and the Al/Si ratio has been varied. The components of some of phase mixtures encountered during the cooling of alloy with Al as 20% wt. of Si are numbered and mentioned alongside the diagram to improve readability

At this temperature, the BCC-A2 contains 64% Cu, 21% Al, 13% Sn, 1.8% Si and 0.2% Fe (by %wt.). For brevity, we would refer this as BBC-A2. At ≈624 °C, Al-Cu binary phase (epsilon) precipitates out from the BCC-A2 solid solution. However, this compound is expected to be stable only until ≈584 °C, when it starts to precipitate Al_9Cu_{11}. As cooling proceeds, the Al and Cu continue to precipitate out of the BCC-A2, and it grows richer in Sn. At ≈531.5°C, the BBC-A2 contains 56% Cu, 26% Sn, 17% Al and 1% Si (%wt.). At this point, the solid alloy begins to melt and results in a liquid3 with 97.5% Sn and 1.8% Cu and 0.7% Al (% wt.). Correspondingly the amount of Al_9Cu_{11} increases by almost 75%. At ≈ 231.5°C, the liquid3 solidifies along with a small amount of Al forming Sn-Al alloy (BCT). At this temperature the solid alloy comprises FeSi, $FeSi_2$, $FeSiAl_2$, Al_9Cu_{11} and the Sn-Al BCT alloy. As cooling further progresses, at ≈148.7°C, $FeSiAl_2$ undergoes a solid-state transformation to $Al_5Fe_2Si_2$.

Simultaneously, the amount of FeSi increases by ≈25% and the $FeSi_2$ decreases in amount by ≈3.5%. As the alloy cools down further, the proportion of $FeSi_2$ continues to reduce further while that of FeSi increases. Finally, at 75 °C, Al_9Cu_{11} undergoes a solid-

state transformation to Al_2Cu_3, accompanied by a decrease in the amounts of $FeSi_2$ and increase in $Al_5Fe_2Si_2$. At 50°C, the alloy comprises 57.5% wt. of $FeSi_2$, 21.5% wt. of FeSi, 15.3% wt. of $Al_5Fe_2Si_2$, 5% wt. of Al_2Cu_3 and 0.7% wt. of Sn-BCT alloy.

3.5.2. FeSi75 alloy made with Al rich recycled silicon

The phase diagram for the FeSi75Al0-25Cu10Sn2 alloy system obtained using FactSage is shown in Fig 15. The composition of the alloy system is given in table 7.

As the alloy cools down from a temperature of 1500°C, it remains as a homogenous liquid until a temperature of ≈1230°C. This is a significant change with respect to earlier discussed FeSi75 alloys with only one impurity (Al or Cu or Sn). When all the three impurities are present, the temperature which marks the onset of crystallization of Si (diamond phase), reduces considerably. For FeSi75Al20, the temperature of onset of solidification was computed to be 1253°C. With the inclusion of Cu and Sn, the temperature of crystallization drops further by ≈23°C. As the alloy cools, Si-Diamond phase continues to precipitate. Si-Diamond phase dissolves Fe, Al and Sn, however Cu does not dissolve in it. In terms of the % wt. of the phase, Sn contributes 0.028% (at 1200°C) to a maximum of 0.036% (at 1098°C) of the total mass of Si diamond phase, which the maximum of all impurities in Si-diamond. At ≈1098°C, Fe_3Si_7 begins to precipitate from the liquid phase. During the process of cooling from 1500 °C, as different phases continue to precipitate from the liquid solution, it gradually becomes richer in Al and Cu.

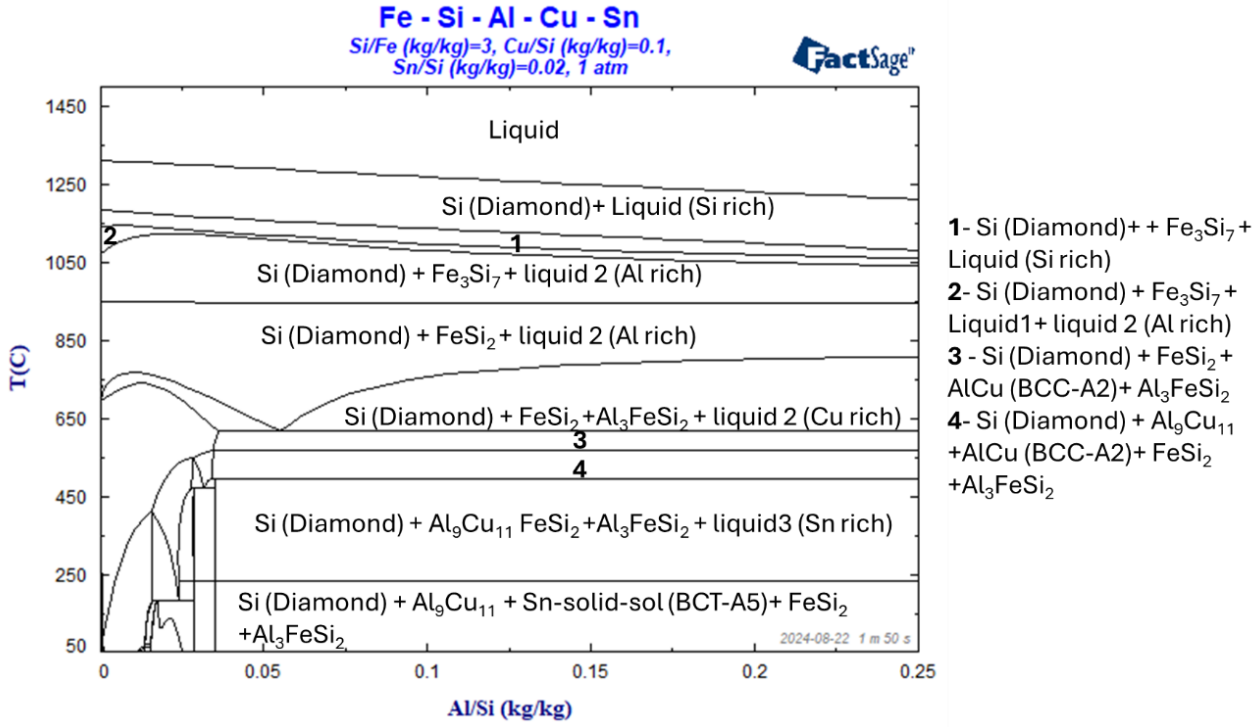

Fig. 15. Phase diagram of FeSi45Al20Cu10Sn2 alloy systems with Al (0-25% wt. of Si), Cu (10% wt. of Si) and Sn (2% wt. of Si) as impurities. In this phase diagram, the ratios Si/Fe, Cu/Si and Sn/Si are kept constants, and the Al/Si ratio has been varied. The components of some of phase mixtures encountered during the cooling of alloy with Al as 20% wt of Si are numbered and mentioned alongside the diagram to improve readability

As seen earlier for FESi45 based alloy, at ≈1069°C, the liquid phase is theoretically considered to be composed of two immiscible solutions, however, the composition of the two solutions is different from those encountered in FeSi45 based alloy. As mentioned earlier, this is probably an artifact of the software, and it relates to the different databases being used to evaluate the alloy composition as it cools down. At ≈1049°C, only liquid2 exists, which now includes the entire mass of copper in liquid phase. As cooling progresses, the liquid loses Fe and Si, while the number of other components remains almost constant. At ≈943°C, the Fe_3Si_7 transforms to $FeSi_2$. With further cooling, the amounts of Si-diamond phase and $FeSi_2$ phase continue to increase with a corresponding decrease of these two components from the liquid solution. At ≈800°C, Al_3FeSi_2 begins to precipitate from the solution. At ≈616°C, the liquid comprises primarily Cu, Al and Sn which make 95% of the solution. At ≈615°C, the remaining liquid solidifies into a BCC solid solution, where Al and Sn are dissolved in Cu. At ≈565°C, a new solid phase of Al_9Cu_{11} is expected to form, with a corresponding decrease in the Al and Cu content from the BCC solution, which is only stable at higher temperatures. As cooling progresses, Al_9Cu_{11} increases in proportion, amounts of Si-diamond and $FeSi_2$ remain fairly stable while that of Al_3FeSi_2 decreases. At ≈495°C, the BCC solid solution becomes rich in Sn and is no longer stable in the solid state. Hence, at this temperature,

the simulations show the reappearance of the liquid3 phase, which now comprises 98% Sn. Finally, at ≈231°C, the liquid3 solidifies to Sn-BCT solid solution dissolving extremely small amount of Al. Finally, at 50°C, the FeSi75 alloy is expected to be composed of 38.1% wt. Si-Diamond phase, 28.7% wt. of Al_3FeSi_2, 23.8% wt. $FeSi_2$, 8.2% wt. Al_9Cu_{11} and 1.2% wt. of Sn-BCT alloy.

3.5.3. FeSi45 alloy made with Cu rich recycled silicon

The composition of the alloy systems made from recycled silicon, originating from the microchips and other consumer electronic gadgets wastes are expected to contain Cu as the main contamination. For this work, we have considered the hypothetical scenario where Si contains 10% wt. Cu and 5% wt. each of Al and Sn as mentioned in Table 7. We will analyse the cooling behaviour for FeSi45A5Cu10Sn5 alloy.

As cooling progresses, the phase diagram shows an appearance of another liquid phase, where Cu is the solvent. This is an artifact of the software as it considers different thermodynamic databases for steel-based solution to those used for non-ferrous based solutions. Hence, the phase diagram shows the concurrent existence of two immiscible liquid phases; one where Fe is in the majority while another where Cu, Al and Sn are in majority, with Fe less than 4% of the entire mass of liquid2. At ≈1098°C, only non-ferrous based liquid2 is remaining as the Fe-based liquid has completely solidified into FeSi and Fe_3Si_7. At ≈994°C, Fe_3Si_7 undergoes a solid-state transformation into to $FeSi_2$. At ≈689°C, $FeSiAl_2$ begins to crystallize out of the Cu rich liquid solution, taking with it the limited amount of Fe and Si remaining in the solution.

It is possible that some Fe and Si also dissolves out of FeSi solid, as the amount of the amounts of $FeSiAl_2$ and $FeSi_2$ increase continuously at the expense of FeSi, which decreases continuously as cooling proceeds. For example, between 689°C and 550°C, the amount of FeSi decreases by 5.7% wt. During the same duration, the amount of $FeSiAl_2$ and $FeSi_2$ increase by 725% (wt.) and 1% wt. respectively. At ≈670°C, Cu based BCC solid solution with Al and tin and extremely small amounts of Fe (0.1% wt.), and Si (1.9% wt.) begins to precipitate out of the liquid solution. As the alloy cools down further, the Cu based BCC solid alloy increases in proportion, incorporating almost entire Cu and Al and >95% Sn from the liquid solution. At ≈531°C, the liquid is primarily composed of Sn (≈97%). At this temperature several changes are expected to occur in the alloy under equilibrium conditions. The Cu based BCC alloy disintegrates and results in the appearance of Al_9Cu_{11}. The Sn incorporated in the BCC solid solution becomes liquid again and remains as a liquid solution. The amount of $FeSiAl_2$ decreases in by 25% (wt.), while those of FeSi and $FeSi_2$ increase by 0.2% and 0.5% wt. respectively. As cooling progresses, the liquid becomes even richer in Sn, as the Al and Cu from the liquid continue to add to the existing amount of Al_9Cu_{11}. At ≈231°C, the liquid is expected to be 99.9% Sn, at which point under equilibrium conditions, the liquid solidifies to Sn based BCT alloy. At ≈148°C, the $FeSiAl_2$ is no longer stable and transforms to $Al_5Fe_2Si_2$, with some part of the $FeSiAl_2$ contributing to the increase in FeSi phase. Finally, at ≈75°C, the Al_9Cu_{11} undergoes a solid-state transformation to Al_2Cu_3 phase. At this temperature, under equilibrium conditions, $Al_5Fe_2Si_2$ also increases in proportion by ≈1.5 times. The additional Fe and Si required to form $Al_5Fe_2Si_2$ is provided by FeSi and $FeSi_2$ phases. Finally, at 50°C, the composition of the alloy in terms of wt% is expected to be 63% $FeSi_2$, 27.6% FeSi, 5.3% Al_2Cu_3, 2.1% Sn-BCT alloy and 2% $Al_5Fe_2Si_2$.

3.5.4. FeSi75 alloy made with Cu rich recycled silicon

The phase diagrams of FeSi75 with Al, Cu and Sn as impurities are shown in figures 17a and 17b. The diagram was calculated by holding constant the Si/Fe, Al/Si and Sn/Si ratios as 3, 0.05 and 0.05 respectively. The percentage of Cu as wt% of Si was varied between 0 and 0.25. In this work, we shall explain the cooling of the FeSi75Al5Cu10Sn5 alloy as mentioned in Table 7.

The alloy remains as a homogenous liquid until ≈1287 °C. At this temperature, Si-diamond phase starts to precipitate from the liquid as solid crystals. The Si-diamond phase is expected to dissolve small amounts of Sn, Al and Fe, which together constitute only 0.1% of the mass of Si-diamond phase at 1250°C. At ≈1154°C, Fe_3Si_7 is the next solid phase to appear. The Fe_3Si_7 phase incorporates some Al in the form of Fe_3Al_7, which contributes within 0.1-0.3 wt% of Fe_3Si_7 phase between 1150 and 945 °C. At ≈1135°C, two different liquid solutions (Liquid and liquid2) are visible in the phase diagram, which as explained earlier is an artefact of the software and is representative of the way calculations are done using different databases. At ≈1112°C, the liquid solution comprises mainly of Cu and Si in equal proportions, along with Al, Sn and Fe. As the alloy cools down, proportion of Si-diamond phase and Fe_3Si_7 phase continue to increase, at the expense of Fe and Si proportions in the liquid phase. As the alloy cools down the solution keeps growing richer in Cu. At ≈945°C, the Fe_3Si_7 undergoes a solid-state transition under equilibrium to $FeSi_2$, while the extra silicon contributes towards the increase in the proportion of Si-Diamond phase. At ≈623°C, a copper-based BCC solid solution begins to crystallize from the Cu rich liquid2. At ≈606°C, Al_3FeSi_2 begins to precipitate from the liquid2 as well. As cooling progresses under equilibrium conditions, the liquid continues to solidify, leading to an increase in the amount of all solid phases. At ≈495°C, under equilibrium conditions, the Cu-BCC solution is no longer stable, and it dissolves, accompanied by the appearance of Al_9Cu_{11} phase. The Sn incorporated in the BCC solid solution now returns to liquid state. The liquid phase is now primarily Sn (99.8% wt.) with small quantities of Al and Cu. As the alloy cools further, at ≈231°C the liquid solution solidifies into Sn-BCT alloy. The Si-Diamond phase loses almost all of its Fe and Al, while Sn remains in amounts less than $1x10^{-5}$% wt. The Sn based BCT alloy incorporates some Al, ≈0.01%wt. As the alloy cools further no further phase transformations occur. The amount of Al_9Cu_{11} remains stable below 231°C. Finally, at 50°C, the alloy comprises 43.1%wt Si-diamond phase, 41.9% wt, $FeSi_2$, 8.8%wt. Al_9Cu_{11}, 3.3%wt. Sn-BCT solid solution and 2.9%wt. Al_3FeSi_2.

The final compositions of the different FeSi45 and FeSi75 alloys made with Al-rich and Cu-rich crystalline Si in shown in Fig. 18 (FeSi45) and Fig 19 (FeSi75) respectively.

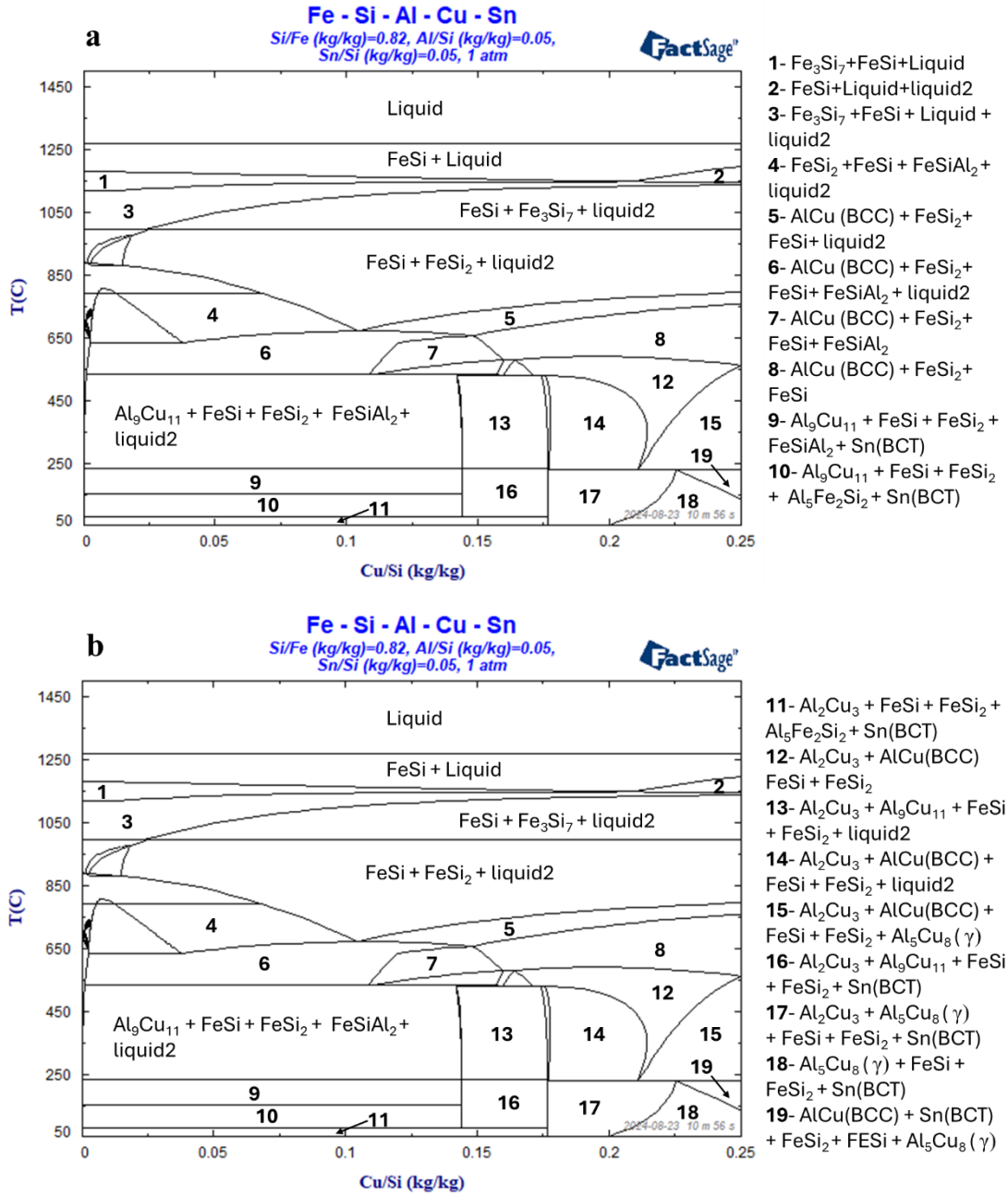

Fig. 16. a and b: Phase diagrams of FeSi45Al5Cu10Sn5 alloy systems with Cu (0-25% wt. of Si), Al (5% wt. of Si) and Sn (5% wt. of Si) as impurities. In this phase diagram, the ratios Si/Fe, Al/Si and Sn/Si are kept constants, and the Cu/Si ratio has been varied. The components of some of phase mixtures encountered during the cooling of alloy with Cu as 10% wt of Si are numbered and mentioned alongside the diagram to improve readability

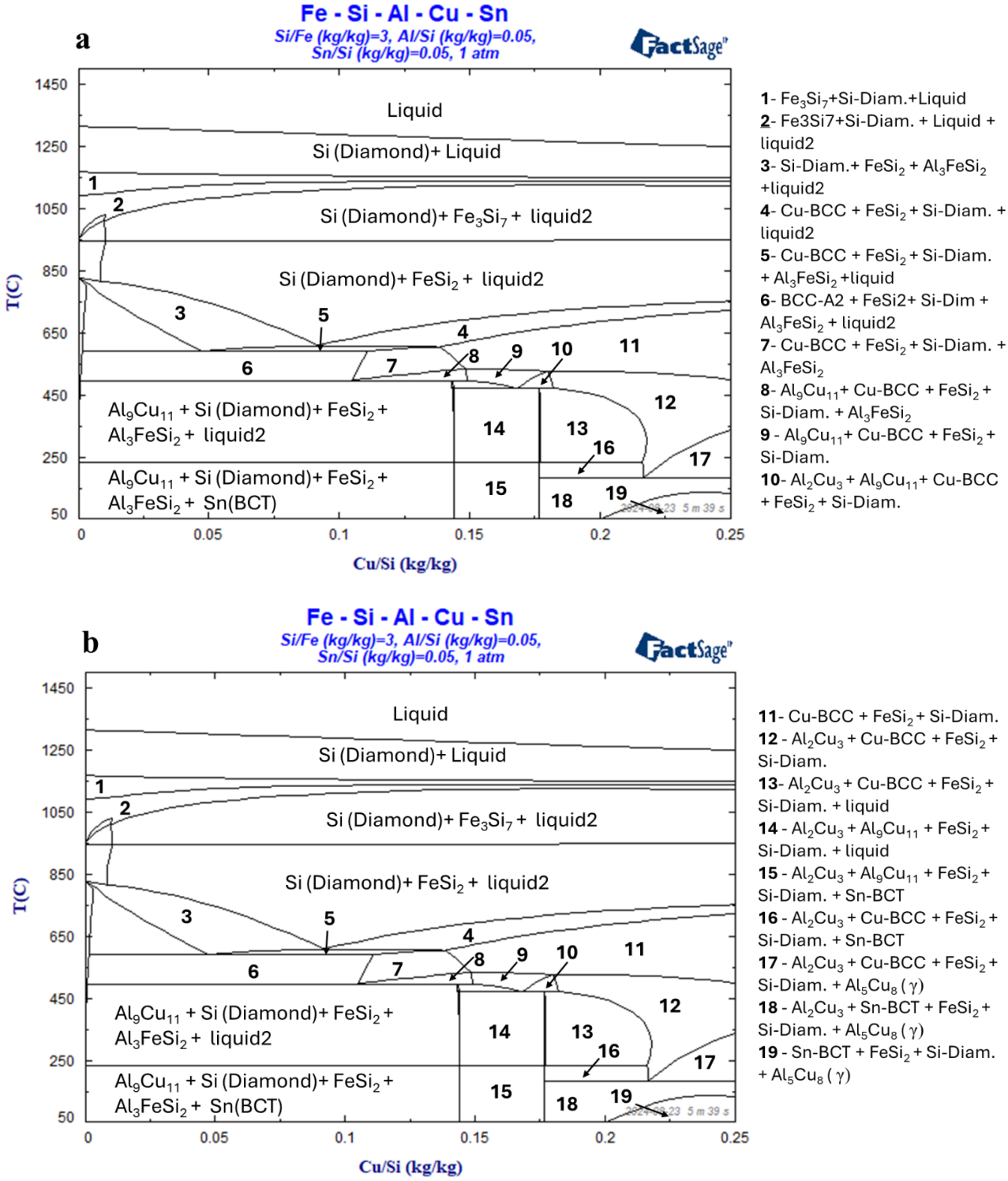

Fig. 17 a and b: Phase diagrams of FeSi75Al5Cu10Sn5 alloys systems with Cu (0-25% wt. of Si), Al (5% wt. of Si) and Sn (5% wt. of Si) as impurities. In this phase diagram, the ratios Si/Fe, Al/Si and Sn/Si are kept constants, and the Cu/Si ratio has been varied. The components of some of phase mixtures encountered during the cooling of alloy with Cu as 10% wt of Si are numbered and mentioned alongside the diagram to improve readability

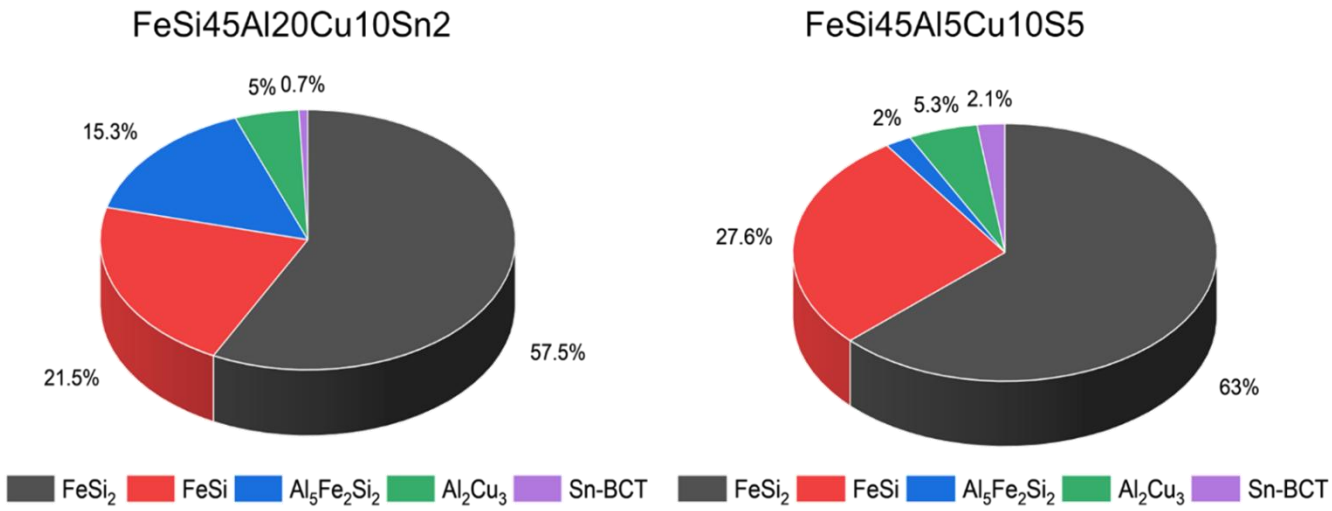

Fig. 18. Pie chart showing the final composition of the FeSi45Al20Cu10Sn2 and FeSi45Al5Cu10Sn5 at 50°C calculated using FactSage under equilibrium solidifcation conditions

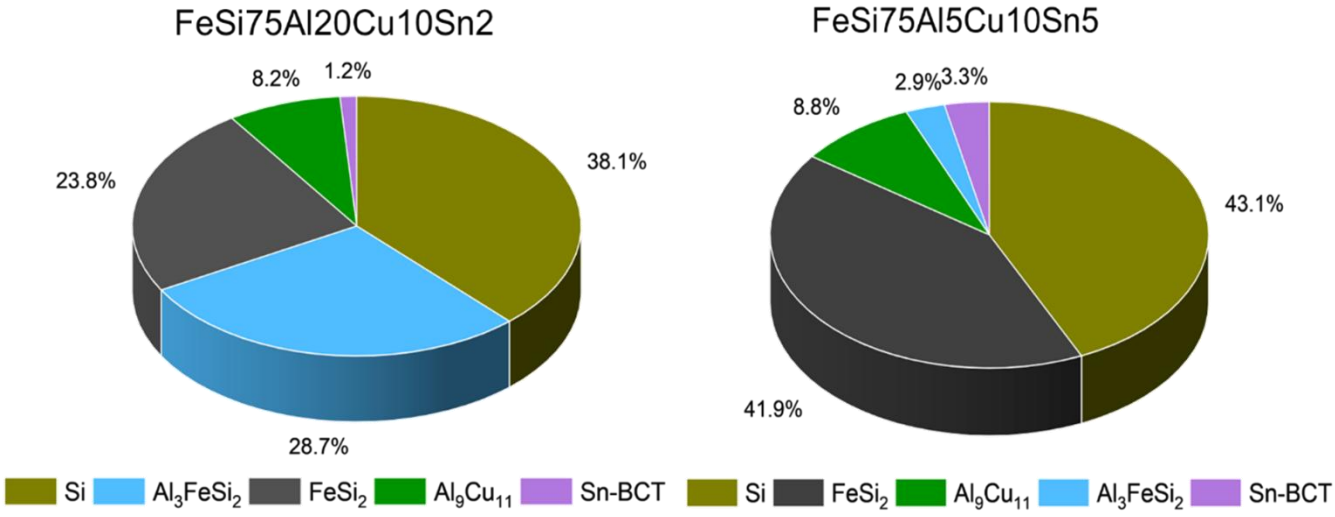

Fig 19: Pie chart showing the final composition of the FeSi75Al20Cu10Sn2 and FeSi75Al5Cu10Sn5 at 50°C calculated using FactSage under equilibrium solidifcation conditions

4. Conclusions

Recycling metal-contaminated Si from e-waste provides a sustainable way to use valuable Si as the raw material. Using Si from e-waste and Fe scrap, FeSi alloys could be produced without using a reducing agent, using only electricity as the source of energy. This could greatly reduce the amount of greenhouse gases generated and the energy consumed in the standard production process of FeSi alloys [4]. Recycled Si from e-waste could contain mainly Al, Cu and Sn as major impurities. In some cases, trace amounts of Ag, Au and other heavy materials may be present. In this work, we presented and discussed the characteristics of FeSi45 and FeSi75 based alloys which were hypothetically prepared with Si from e-waste. FeSi alloys with different compositions of recycled silicon were considered to simulate the resulting FeSi alloys. In this work two FeSi alloy systems (FeSi45 and FeSi75) and three impurities (Al, Cu and Sn) were analysed. The impurities were considered as the 5 wt. of Si, as this is expected to be the practical situation in real-world applications. First the impact of the individual contaminant in Si was analysed, followed by the analysis of system with all three contaminants present simultaneously, as is expected in practical applications. Considering the theoretical simulations, some areas of importance for applications of such alloys could be identified.

The temperature above which the alloy completely exists as a homogeneous liquid phase changes with the addition of the impurities. This is important for several uses of FeSi such as

alloying and deoxidizing. If the melting temperature is not sufficiently high, the FeSi alloy may not melt completely and hence may remain underutilized. Additionally, solid pieces of FeSi may appear as inclusions in the final product. The appropriate liquidation temperature of the alloy should be known for controlling the intended performance of the FeSi alloys.

The amount of energy required for melting the alloy is also expected to change with the inclusion of impurities. Theoretically, the more the number of endothermic phase changes in an alloy, the higher is the change in entropy and more energy is required to support those phase changes. While cooling, according to the calculations, all the phase changes in different alloy systems were exothermic in nature. Hence, while heating up the alloy all the accompanying phase changes would become endothermic in nature. However, the actual amount of energy required would depend on the number of different phases present in the FeSi being used and the rate of heating. Since, in most metallurgical operations the heating rate is extremely high, most phase changes at lower temperatures are not expected to proceed to completion.

The theory of solidification for such complex alloys systems involving eutectic and peritectic reactions has been explained in published literature. Upon finer inspection of the equilibrium solidification process, it is possible to express the ending point of equilibrium solidification and solute redistribution path in terms of solute concentration [66]. Furthermore, the formation of intermetallic compounds as a result of peritectic transformations in the presence of more than one impurities can further described theoretically with the help of partition ratio, which can either considered to be constant or varying [67]. It has been known that the primary phase involved in a peritectic reaction can be consumed either partially or completely during the peritectic reaction depending on the value of the solidification rate [67]. These calculations require rigorous mathematical calculations, considering Scheil's model [66,67], and could be performed in a future work to improve the understanding of the complex solidification process in such alloys with multiple impurities.

The phases present in the FeSi alloy prepared with recycled Si from electronic waste, will depend largely on the composition of the Si and the cooling rate of the FeSi alloy. In most cases, the FeSi alloy is air-cooled with natural ventilation [4]. Hence, the exact amount of phases present would depend on the kinetics of such phase changes, the determination of which is beyond the scope of this work. Nevertheless, the presence of additional phases may alter the mechanical properties of the FeSi alloy. This could impact the material handling and preparation of the FeSi alloy for metallurgical uses. For example, the crushing behaviour of the FeSi alloy will change depending on the proportion of soft or brittle alloy phases present in the FeSi alloy being used. To determine the impact of such additional phases formed due to the impurities contained in the recycled Si, further experimental studies are required. Nevertheless, this work provides a framework and basis for carrying out such experimental studies to understand the impact of multicomponent FeSi alloys and their use in the metallurgical industries.

Acknowledgements

This research is part of the project No. 2022/45/P/ST5/02712, co-funded by the National Science Centre and the European Union Framework Programme for Research and Innovation Horizon 2020 under the Marie Skłodowska-Curie grant agreement No. 945339. For the purpose of Open Access, the author has applied a CC-BY public copyright license to any Author Accepted Manuscript (AAM) version arising from this submission

References

[1] L. Riva, G.R. Surup, T.V. Buø, H.K. Nielsen, (2019) . A study of densified biochar as carbon source in the silicon and ferrosilicon production, Energy 181 985–996. https://doi.org/10.1016/j.energy.2019.06.013.

[2] M. Tangstad, J.P. Beukes, J. Steenkamp, E. Ringdalen, (2019) Coal-based reducing agents in ferroalloys and silicon production, in: New Trends in Coal Conversion, Elsevier,: pp. 405–438. https://doi.org//10.1016/B978-0-08-102201-6.00014-5.

[3] A.N. Ismail, M.H. Ibrahim, R.M. Said, F. Somidin, S.A. Ismail, (2022) Influence of recycled wastes on ferrosilicon production in steel making applications: A short review, in: J Phys Conf Ser, IOP Publishing,: p. 012028. https://doi.org/10.1088/1742-6596/2169/1/012028.

[4] M. Tangstad, (2013) Ferrosilicon and silicon technology, in: Handbook of Ferroalloys, Elsevier,: pp. 179–220. https://doi.org/10.1016/B978-0-08-097753-9.00006-X.

[5] R. Farzana, V. Sahajwalla, (2015). Novel recycling to transform automotive waste glass and plastics into SiC-bearing resource by silica reduction, Journal of Sustainable Metallurgy 1 65–74. https://doi.org/10.1007/s40831-014-0004-2.

[6] R. Farzana, R. Rajarao, V. Sahajwalla, (2014) . Transforming waste plastic into reductants for synthesis of ferrosilicon alloy, Ind Eng Chem Res 53 19870–19877. https://doi.org/10.1021/ie5041513.

[7] R. Farzana, R. Rajarao, V. Sahajwalla, (2013). Synthesis of ferrosilicon alloy using waste glass and plastic, Mater Lett 116,101–103. https://doi.org/10.1016/j.matlet.2013.10.105.

[8] R. Farzana, R. Rajarao, V. Sahajwalla, (2016). Characteristics of waste automotive glasses as silica resource in ferrosilicon synthesis, Waste Management & Research 34 113–121. https://doi.org/10.1177/0734242X15617010.

[9] R. Farzana, R. Rajarao, V. Sahajwalla, (2017). Reaction mechanism of ferrosilicon synthesis using waste plastic as a reductant, ISIJ International 57 1780–1787. https://doi.org/10.2355/isijinternational.ISIJINT-2017-199.

[10] R. Rajarao, R. Farzana, V. Sahajwalla, (2018). Transforming waste printed circuit boards and compact discs for the synthesis of valuable ferrosilicon alloy, Journal of Sustainable Metallurgy 4 461–469. https://doi.org/10.1007/s40831-018-0194-0.

[11] M.P. Kuz'min, P.K. Chu, A.M. Qasim, L.M. Larionov, M.Y. Kuz'mina, P.B. Kuz'min, (2019). Obtaining of Al–Si foundry alloys using amorphous microsilica–Crystalline silicon production waste, J Alloys Compd 806 806–813. https://doi.org/10.1016/j.jallcom.2019.07.312.

[12] L. Blaesing, A. Walnsch, S. Hippmann, C. Modrzynski, C. Weidlich, S. Pavón, M. Bertau, (2024). Ferrosilicon Production from Silicon Wafer Breakage and Red Mud, ACS Sustainable Resource Management 1 404–416. https://doi.org/10.1021/acssusresmgt.3c00035.

[13] F. Ardente, C.E.L. Latunussa, G.A. Blengini, (2019). Resource efficient recovery of critical and precious metals from waste silicon PV panel recycling, Waste Management 91 156–167. https://doi.org/10.1016/j.wasman.2019.04.059.

[14] X. Wang, X. Tian, X. Chen, L. Ren, C. Geng, (2022). A review of end-of-life crystalline silicon solar photovoltaic panel recycling technology, Solar Energy Materials and Solar Cells 248 111976. https://doi.org/10.1016/j.solmat.2022.111976.

[15] J. Cui, L. Zhang, (2008). Metallurgical recovery of metals from electronic waste: A review, J Hazard Mater 158 228–256. https://doi.org/10.1016/j.jhazmat.2008.02.001.

[16] C. Latunussa, L. Mancini, G. Blengini, F. Ardente, D. Pennington, (2016). Analysis of material recovery from silicon photovoltaic panels, JRC Publications Repository JRC100783. https://doi.org/10.2788/786252.

[17] P. Padhamnath, J.K. Buatis, A. Khanna, N. Nampalli, N. Nandakumar, V. Shanmugam, A.G. Aberle, S. Duttagupta, (2020). Characterization of screen printed and fire-through contacts on LPCVD based passivating contacts in monoPoly™ solar cells, Solar Energy 202 73–79. https://doi.org/10.1016/j.solener.2020.03.087.

[18] S.P. Gupta, (2002). Intermetallic compound formation in Fe–Al–Si ternary system: Part I, Mater Charact 49 269–291. https://doi.org/10.1016/S1044-5803(03)00006-8.

[19] Z.-K. Liu, Y.A. Chang, (1999). Thermodynamic assessment of the Al-Fe-Si system, Metallurgical and Materials Transactions A 30 1081–1095. https://doi.org/10.1007/s11661-999-0160-3.

[20] M. Fukaya, T. Miyazaki, T. Kozakai, (1991). Phase diagrams calculated for Fe-rich Fe-Si-Co and Fe-Si-Al ordering alloy systems, J Mater Sci 26 5420–5426. https://doi.org/10.1007/BF02403939.

[21] A.A. Akberdin, A.S. Kim, A.S. Orlov, R.B. Sultangaziev, (2022). Diagram of the phase composition of the Fe–Si–Al system and its isothermal sections, CIS Iron Steel Rev 23 76–80.

[22] K. Nová, P. Novák, F. Průša, J. Kopeček, J. Čech, (2018). Synthesis of intermetallics in Fe-Al-Si system by mechanical alloying, Metals (Basel) 9 20. https://doi.org/10.3390/met9010020.

[23] Z. Tsakadze, L.P. Tan, K.P. Davidson, S. Gorsse, V. Chaudhary, R. V Ramanujan, (2024). Accelerated multi-property discovery of promising Fe-Si-Al magnetic alloys, Materialia (Oxf) 36 102168. https://doi.org/10.1016/j.mtla.2024.102168.

[24] C. Zhang, Y. Chen, S. Feng, X. Kan, Y. Zhu, Y. Li, W. Sun, J. Shen, X. Liu, (2023). Improvement of electromagnetic properties of FeSiAl soft magnetic composites, J Mater Sci 58 9698–9707. https://doi.org/10.1007/s10853-023-08610-4.

[25] B. Zuo, N. Saraswati, T. Sritharan, H.H. Hng, (2004). Production and annealing of nanocrystalline Fe–Si and Fe–Si–Al alloy powders, Materials Science and Engineering: A 371 210–216. https://doi.org/10.1016/j.msea.2003.11.046.

[26] T. Wakiyama, M. Takahashi, S. Nishimaki, J. Shimoda, (1981). Magnetic properties of Fe-Si-Al single crystals, IEEE Trans Magn 17, 3147–3150. https://doi.org/10.1109/TMAG.1981.1061694.

[27] S.G. Shabestari, (1994) Formation of iron-bearing intermetallics in aluminum-silicon casting alloys, McGill University, Montreal, Quebec, Canada,.

[28] X. Li, Z. Li, (2017) Experimental investigation of the 650° C isothermal section of the Cu-Fe-Si ternary phase diagram, J Phase Equilibria Diffus 38 94–101. https://doi.org/10.1007/s11669-017-0519-x.

[29] M. Heuer, T. Buonassisi, A.A. Istratov, M.D. Pickett, M.A. Marcus, A.M. Minor, E.R. Weber (2007), Transition metal interaction and Ni-Fe-Cu-Si phases in silicon, J Appl Phys 101. https://doi.org/10.1063/1.2748346.

[30] P.H. Wu, N. Liu, Z.X. Zhu, (2015). Liquid-phase separation of undercooled Fe-Cu-Si alloy, Adv Mat Res 1095 160–163. https://doi.org/10.4028/www.scientific.net/amr.1095.160.

[31] I. Yamauchi, T. Irie, H. Sakaguchi, (2005). Metastable liquid separation in undercooled Fe–Cu and Fe–Cu–Si melts containing a small B concentration and their solidification structure, J

Alloys Compd 403 211–216. https://doi.org/10.1016/j.jallcom.2005.05.031.
[32] I. Yamauchi, H. Okamoto, A. Suganuma, I. Ohnaka, (1998). Effects of Cu addition on the β-phase formation rate in Fe2Si5 thermoelectric materials, J Mater Sci 33 385–394. https://doi.org/10.1023/A:1004323930521.
[33] T. Kataoka, Y. Arita, F. Takahashi, H. Fujimura, Y. Kurosaki, M. Sugiyama, I. Ohnuma, (2016). Precipitation Behavior of Copper Sulfides in Fe–Si–Cu–S Ferritic Steel, ISIJ International 56 2062–2067. https://doi.org/10.2355/isijinternational.ISIJINT-2016-056.
[34] X. Wang, B. Zhou, Z. Guo, Y. Liu, J. Wang, X. Su, (2017). Experimental investigation and thermodynamic calculation of the Fe–Si–Sn system, Calphad 57 88–97. https://doi.org/10.1016/j.calphad.2017.03.006.
[35] Y. Liu, F. Yin, J. Hu, L.I. Zhi, S. Cheng, (2018). Phase equilibria of Al–Fe–Sn ternary system, Transactions of Nonferrous Metals Society of China 28 282–289. https://doi.org/10.1016/S1003-6326(18)64661-8.
[36] J.G. Li, W.J. Yuan, Y. Zhou, L.M. Zhang, (2008). Effect of Sn on the Sintering of Fe-Si Alloys, Key Eng Mater 368 1591–1592. https://doi.org/10.4028/www.scientific.net/KEM.368-372.1591.
[37] W. Wołczyński, (2020). Pattern Selection in the Eutectic Growth-Thermodynamic Interpretation, Archives of Metallurgy and Materials 65 653–666. https://doi.org/10.24425/amm.2020.132804.
[38] C. Yang, Q. Tan, L. Liu, Q. Dong, J. Li, (2017). Recycling tin from electronic waste: a problem that needs more attention, ACS Sustain Chem Eng 5 9586–9598. https://doi.org/10.1021/acssuschemeng.7b02903.
[39] R.V. Sapinov, M.A. Sadenova, N.A. Kulenova, N.V. Oleinikova, (2020). Improving Hydrometallurgical Methods for Processing Tin-containing Electronic Waste., CET Journal-Chemical Engineering Transactions 81. https://doi.org/10.3303/CET2081171.
[40] J.A. Barragan, C. Ponce de León, J.R. Alemán Castro, A. Peregrina-Lucano, F. Gómez-Zamudio, E.R. Larios-Durán, (2020). Copper and antimony recovery from electronic waste by hydrometallurgical and electrochemical techniques, ACS Omega 5 12355–12363. https://doi.org/10.1021/acsomega.0c01100.
[41] P. Jadhao, G. Chauhan, K.K. Pant, K.D.P. Nigam, (2016). Greener approach for the extraction of copper metal from electronic waste, Waste Management 57 102–112. https://doi.org/10.1016/j.wasman.2015.11.023.
[42] R. Sinha, G. Chauhan, A. Singh, A. Kumar, S. Acharya, (2018). A novel eco-friendly hybrid approach for recovery and reuse of copper from electronic waste, J Environ Chem Eng 6 1053–1061. https://doi.org/10.1016/j.jece.2018.01.030.
[43] P. Padhamnath, M. Ślęzak, M. Karbowniczek, (2023) Disposing End of Life PV Modules – Reusing, Recycling and Upcycling, in: EU PVSEC 2023, EUPVSEC, Lisbon, Portugal,: pp. 001–008. https://doi.org/10.4229/EUPVSEC2023/5DV.2.62.
[44] A.K. Pahari, B.K. Dubey, (2019) Waste from electrical and electronics equipment, in: Plastics to Energy, Elsevier: pp. 443–468. https://doi.org/10.1016/B978-0-12-813140-4.00018-2.
[45] M. Littmann, (1971). Iron and silicon-iron alloys, IEEE Trans Magn 7 48–60. https://doi.org/10.1109/TMAG.1971.1066998.
[46] T.I. Sigfússon, Ö. Helgason, (1990). Rates of transformations in the ferrosilicon system, Hyperfine Interact 54 861–867. https://doi.org/10.1007/BF02396141.
[47] A. Gilbert, W.S. Owen, (1962). Diffusionless transformation in iron-nickel, iron-chromium and iron-silicon alloys, Acta Metallurgica 10 45–54. https://doi.org/10.1016/0001-6160(62)90185-2.
[48] Q.C. Hom, C.L. Nassaralla, (1998). R.W. Heckel, Microstructural Study of Granulated Ferrosilicon with 75wt% Silicon, in: The Proceedings of ·/NFACON 8, Beijing,. https://www.pyrometallurgy.co.za/InfaconVIII/126-Horn.pdf (accessed January 18, 2025).
[49] S. Tomé-Torquemada, B. Glaser, K. Hildal, D. Sichen, (2017). Experimental Study on the Activities of Al and Ca in Ferrosilicon, Metallurgical and Materials Transactions B 48 3251–3258. https://doi.org/10.1007/s11663-017-1119-1.
[50] O. Krause, H. Ryssel, P. Pichler, (2002). Determination of aluminum diffusion parameters in silicon, J Appl Phys 91 5645–5649. https://doi.org/10.1063/1.1465501.
[51] Y.-M. Kim, S.-W. Choi, S.-K. Hong, (2016). The behavior of thermal diffusivity change according to the heat treatment in Al-Si binary system, J Alloys Compd 687 54–58. https://doi.org/10.1016/j.jallcom.2016.06.080.
[52] J.O. McCaldin, H. Sankur, (1971). Diffusivity and solubility of Si in the Al metallization of integrated

circuits, Appl Phys Lett 19 524–527. https://doi.org/10.1063/1.1653799.
[53] F.J. Blatt, (1955). Effect of point imperfections on the electrical properties of copper. I. Conductivity, Physical Review 99 1708. https://doi.org/10.1103/PhysRev.99.1708.
[54] S.P. Murarka, (2001). Materials aspects of copper interconnection technology for semiconductor applications, Materials Science and Technology 17 749–758. https://doi.org/10.1179/026708301101510564.
[55] A. Lennon, J. Colwell, K.P. Rodbell, (2019). Challenges facing copper-plated metallisation for silicon photovoltaics: Insights from integrated circuit technology development, Progress in Photovoltaics: Research and Applications 27 67–97. https://doi.org/10.1002/pip.3062.
[56] A. Mondon, M.N. Jawaid, J. Bartsch, M. Glatthaar, S.W. Glunz, (2013). Microstructure analysis of the interface situation and adhesion of thermally formed nickel silicide for plated nickel–copper contacts on silicon solar cells, Solar Energy Materials and Solar Cells 117 209–213. https://doi.org/10.1016/j.solmat.2013.06.005.
[57] A. Kraft, C. Wolf, J. Bartsch, M. Glatthaar, S. Glunz, (2015). Long term stability of copper front side contacts for crystalline silicon solar cells, Solar Energy Materials and Solar Cells 136 25–31. https://doi.org/https://doi.org/10.1016/j.solmat.2014.12.024.
[58] A.A. Istratov, E.R. Weber, (2002). Physics of Copper in Silicon, J Electrochem Soc 149 G21. https://doi.org/10.1149/1.1421348.
[59] A.A. Istratov, C. Flink, H. Hieslmair, S.A. McHugo, E.R. Weber, (2000). Diffusion, solubility and gettering of copper in silicon, Materials Science and Engineering: B 72 99–104. https://doi.org/https://doi.org/10.1016/S0921-5107(99)00514-0.
[60] K. Joshi, P. Padhamnath, U. Bhandarkar, S.S. Joshi, (2019). Surface quality and contamination on Si wafer surfaces sliced using wire-electrical discharge machining, J Eng Mater Technol 141 041013. https://doi.org/10.1115/1.4044374.
[61] E. Haccuria, P. Ning, H. Cao, P. Venkatesan, W. Jin, Y. Yang, Z. Sun, (2017) Effective treatment for electronic waste-Selective recovery of copper by combining electrochemical dissolution and deposition, J Clean Prod 152 150–156. https://doi.org/10.1016/j.jclepro.2017.03.112.
[62] G. Salje, M. Feller-Kniepmeier, (1977). The diffusion and solubility of copper in iron, J Appl Phys 48 1833–1839. https://doi.org/10.1063/1.323934.
[63] G. Salje, M. Feller-Kniepmeier, The diffusion and solubility of iron in copper, J Appl Phys 49 (1978) 229–232. https://doi.org/10.1063/1.323934.
[64] R.W. Olesinski, G.J. Abbaschian, (1984) The Si− Sn (silicon− tin) system, Bulletin of Alloy Phase Diagrams 5 273–276. https://doi.org/10.1007/BF02868552.
[65] W.F. Ehret, A.F. Westgren, (1933). X-ray analysis of iron-tin alloys, J Am Chem Soc 55 1339–1351.
[66] W. Wołczyński, (2015). Back-diffusion in crystal growth. Eutectics, Archives of Metallurgy and Materials 60. https://doi.org/10.1515/amm-2015-0392.
[67] W. Wołczyński, (2015). Back-Diffusion In Crystal Growth. Peritectics, Archives of Metallurgy and Materials 60 2409–2414. https://doi.org/10.1515/amm-2015-0393.